remote sensing

MDPI

Article

Evaluating the Relationship Between Vegetation Status and Soil Moisture in Semi-Arid Woodlands, Central Australia, Using Daily Thermal, Vegetation Index, and Reflectance Data

Mauro Holzman [1,2], Ankur Srivastava [2,*], Raúl Rivas [3] and Alfredo Huete [2]

[1] Consejo Nacional de Investigaciones Científicas y Técnicas, Instituto de Hidrología de Llanuras "Dr. Eduardo Jorge Usunoff" (IHLLA), Rep. Italia 780, Azul B7300, Argentina; m.holzman@ihlla.org.ar
[2] Faculty of Science, University of Technology Sydney, Sydney, NSW 2007, Australia; alfredo.huete@uts.edu.au
[3] Comisión de Investigaciones Científicas de la Provincia de Buenos Aires, Instituto de Hidrología de Llanuras "Dr. Eduardo Jorge Usunoff" (IHLLA), Tandil B7000, Argentina; rrivas@rec.unicen.edu.ar
* Correspondence: ankursrivastava117@gmail.com

Abstract: Wet rainfall pulses control vegetation growth through evapotranspiration in most dryland areas. This topic has not been extensively analyzed with respect to the vast semi-arid ecosystems of Central Australia. In this study, we investigated vegetation water responses to in situ root zone soil moisture (SM) variations in savanna woodlands (Mulga) in Central Australia using satellite-based optical and thermal data. Specifically, we used the Land Surface Water Index (LSWI) derived from the Advanced Himawari Imager on board the Himawari 8 (AHI) satellite, alongside Land Surface Temperature (LST) from MODIS Terra and Aqua (MOD/MYD11A1), as indicators of vegetation water status and surface energy balance, respectively. The analysis covered the period from 2016 to 2021. The LSWI increased with the magnitude of wet pulses and showed significant lags in the temporal response to SM, with behavior similar to that of the Enhanced Vegetation Index (EVI). By contrast, LST temporal responses were quicker and correlated with daily in situ SM at different depths. These results were consistent with in situ relationships between LST and SM, with the decreases in LST being coherent with wet pulse magnitude. Daily LSWI and EVI scores were best related to subsurface SM through quadratic relationships that accounted for the lag in vegetation response. Tower flux measures of gross primary production (GPP) were also related to the magnitude of wet pulses, being more correlated with the LSWI and EVI than LST. The results indicated that the vegetation response varied with SM depths. We propose a conceptual model for the relationship between LST and SM in the soil profile, which is useful for the monitoring/forecasting of wet pulse impacts on vegetation. Understanding the temporal changes in rainfall-driven vegetation in the thermal/optical spectra associated with increases in SM can allow us to predict the spatial impact of wet pulses on vegetation dynamics in extensive drylands.

Keywords: land surface temperature; land surface water index; short-wave infrared; vegetation status; wet pulse

Academic Editor: Clement Atzberger

Received: 31 December 2024
Revised: 4 February 2025
Accepted: 11 February 2025
Published: 13 February 2025

Citation: Holzman, M.; Srivastava, A.; Rivas, R.; Huete, A. Evaluating the Relationship Between Vegetation Status and Soil Moisture in Semi-Arid Woodlands, Central Australia, Using Daily Thermal, Vegetation Index, and Reflectance Data. *Remote Sens.* **2025**, *17*, 635. https://doi.org/10.3390/rs17040635

1. Introduction

Dryland ecosystems cover about 40% of the global land area and have an important impact on the inter-annual variability of carbon cycles at a global scale. Extreme events produce fluctuations in vegetation productivity according to water availability for plant use (i.e., evapotranspiration or ET). Different authors have reported that the amount of

precipitation during wet pulses is important for vegetation growth and productivity, with this having a key role in carbon uptake [1–4]. Australia is one of the major dryland areas worldwide. Refs. [5,6] reported the high sensitivity of extensive Central Australian drylands to hydroclimatic variability and thus the vulnerability to predicted future changes in climate.

Semi-arid ecosystems are exposed to sporadic events of intense rainfall. Although rainfall is the main trigger of vegetation response during these events, the water balance in the soil can vary spatio-temporally depending on several factors, such as rainfall intensity, topography, and soil type, among others. Thus, soil moisture (SM) is considered a critical factor in rainfall-driven dryland ecosystems, as a hydrological variable resulting from the water balance in the soil [7–10]. It is a more comprehensive variable than rainfall; thus, it is related to different processes of the soil–plant–atmosphere interface and can subsequently be considered a variable with fewer errors than different factors separately. For example, [11] showed that the Enhanced Vegetation Index (EVI) and solar-induced chlorophyll fluorescence (SIF) were better correlated with surface SM (0–10 cm depth) than precipitation in semi-arid areas of Central Australia. Given that this is a key surface variable of the evapotranspiration process (ETa), the understanding of soil water effect on vegetation dynamics through satellite data can contribute to spatially predicting the response of vegetation to wet pulses in large drylands with limited field measurements [11]. Although surface SM can be retrieved from well-known methods like microwave retrieval algorithms, it may not be enough to determine water vegetation conditions, given the frequent decoupling with deeper depths and given that plants can extract water from subsurface horizons depending on the development of deep roots [11,12]. Moreover, the response of vegetation to root-zone soil water availability has not been extensively analyzed, probably due to the lack of estimates of vertical SM distribution and accessibility of vegetation to it [13].

Australia is one of the largest land masses covered by arid and semi-arid ecosystems, with about 70% of the area represented by woodlands, savannas, and grasslands [14]. The importance of Australian semi-arid ecosystems on global land carbon sink related to changes produced by wet rainfall pulses (typically more than 50 mm/week) has been reported [15]. In 2010–2011, almost 60% of the large global carbon sink anomaly occurred in Australia as a consequence of extraordinary rainfall events [1,3]. In this sense, Mulga (*Acacia* spp.) covers 20–25% of the Australian land area [16] and was one of the most important semi-arid ecosystems contributing to the 2011 carbon sink anomaly [17]. Although it is clear that vegetation growth is strongly associated with wet rainfall events in these semi-arid systems [5,18], the study of the temporal response of vegetation is still important for predicting the impact of those events and to evaluate the performance of different indicators.

Given that SM has spatial and temporal variability, satellite remote sensing offers an opportunity to monitor its impact on vegetation at different spatio-temporal scales. In this sense, geostationary (GEO) satellites have certain advantages over low-Earth-orbiting (LEO) satellites, given the consistency in viewing geometry (which can produce variability in reflectance data), better temporal coverage, and more chances to conduct cloud-free observations [19]. For example, [20] reported that seasonal changes in viewing and illumination geometry could produce significant variations in vegetation indices over Australian woodland and open forest areas. In these drylands, where vegetation can show sub-fortnightly changes as a consequence of rainfall events [21], GEO satellites, such as the recent Japanese Himawari-8, have the potential to monitor those short-time changes.

In Australia, several remote sensing studies have used vegetation indices to monitor productivity and phenology changes, reporting differences in the timing, magnitude, and

duration of vegetation response according to hydrological variability [11,19,22,23]. In general, these studies, at coarse temporal scales, reported certain lags between rainfall events and an increase in the indices, suggesting limitations for the early monitoring of the impact of those events. Other spectral bands, such as short-wave infrared (SWIR) and thermal infrared (TIR), have been less explored in semi-arid Australian areas. Spectral indices such as the Land Surface Water Index (LSWI), which take into account near-infrared (NIR) and SWIR bands, have been widely associated with vegetation water content and vegetation water stress, given the absorption of liquid water in SWIR [24–26]. They can be an alternative to traditional vegetation indices. However, the temporal response in semi-arid, natural regions to rainfall wet pulses has scarcely been explored. It should be noted that, for a certain rainfall pulse, spectral indices can show different values during a season with different general hydrological conditions (e.g., normal or dry seasons).

On the other hand, thermal data have been considered to study the vegetation status based on the partitioning of incoming solar radiation into latent (ET) and sensible heat fluxes under different levels of soil water available for ET [27]. The estimation of vegetation water status is based on the following simplified surface energy balance equation:

$$Rn = LE + H + G \quad (1)$$

where Rn is the net radiation, LE is the latent heat flux, H is the sensible heat flux, and G is the soil heat flux (G is almost equal to 0 over maximum vegetation cover). All these terms are expressed in w m^{-2}. Different variables are associated with LST. First, incoming solar radiation is one of the main drivers [27]. Atmospheric water demand and surface roughness control the flux of heat from the surface to the atmosphere [28]. Thus, potential ET is mainly related to radiative and atmospheric factors. ETa is a key variable determining LST through the surface energy balance depending on changes in SM. LST has been widely used as a simple indicator of vegetation water status, given that, over vegetated areas, the distribution of incoming solar radiation into H and LE mainly depends on stomatal resistance to respiration. For a region under homogeneous atmospheric forcing and surface roughness, LST is strongly related to SM in the root zone available for the ET process [27,29–31]. In this context, changes in LST should be associated not only with surface SM but also with deep SM, depending on vertical root distribution and the sensitivity of the vegetation to that variable [12,30]. These concepts have scarcely been applied to monitor dryland natural areas of Central Australia.

This study aimed to analyze the vegetation response to in situ root zone SM during wet rainfall events in an area of Mulga savanna woodland in Central Australia through LSWI and LST data from AHI Himawari 8 and the Moderate Resolution Imaging Spectroradiometer (MODIS), respectively. The novelty of this study lies in its identification of a satellite-derived indicator of vegetation status, which is related to root zone SM increases during wet rainfall events. Given the scarcely explored potential of this variable to monitor and predict its impact on vegetation [12], an early proxy associated with increases in water in the soil profile can provide a source for monitoring and predicting vegetation condition and productivity. This will contribute to the understanding and spatial monitoring of wet pulse impact on vegetation in the complex semi-arid systems of that region with limited spatial data coverage. The sections are organized as follows: Section 2 includes a description of the study area, field data considered from the Ozflux network, and optical/thermal satellite data; Section 3 includes an analysis of the relationships between SM, GPP, and LSWI/LST data, including a conceptual model of those relationships for the study area.

2. Materials and Methods

2.1. Study Area

This study was carried out at Alice Springs Mulga (ASM) and Ti Tree Ozflux stations, which are located in the Northern Territory, over a homogeneous Mulga woodland (ASM: −22.2828, 133.2493; Ti Tree: −22.2870, 133.6400) [11,32] (Figure 1). Both sites are part of the Terrestrial Ecosystem Research Network's (TERN) OzFlux and Australian SuperSite networks that allow for the monitoring of land surface processes in Australia (https://www.ozflux.org.au/monitoringsites/alicesprings/index.html#intro; https://www.ozflux.org.au/monitoringsites/titreeeast/index.html#intro, accessed on 18 December 2024). These stations were selected since they are the only two existing in the Mulga woodland area. ASM was considered as the primary reference site, given that there is a lack of field data between 1 January 2020 and 19 November 2020 in the Ti Tree station. This last site was considered mainly to corroborate the relationship between variables. The mean annual rainfall is 312 mm (1987–2015) (http://www.bom.gov.au/, accessed on 18 December 2024), ranging from 25 to 955 mm [33]. In total, 86% of rainfall occurs between November and April [14]. Mean minimal and maximal air temperatures are between 5 °C and 22.6 °C (July) and between 22 °C and 37.5 °C (January), respectively, with absolute values between −4 °C (August) and 46 °C (January) [14].

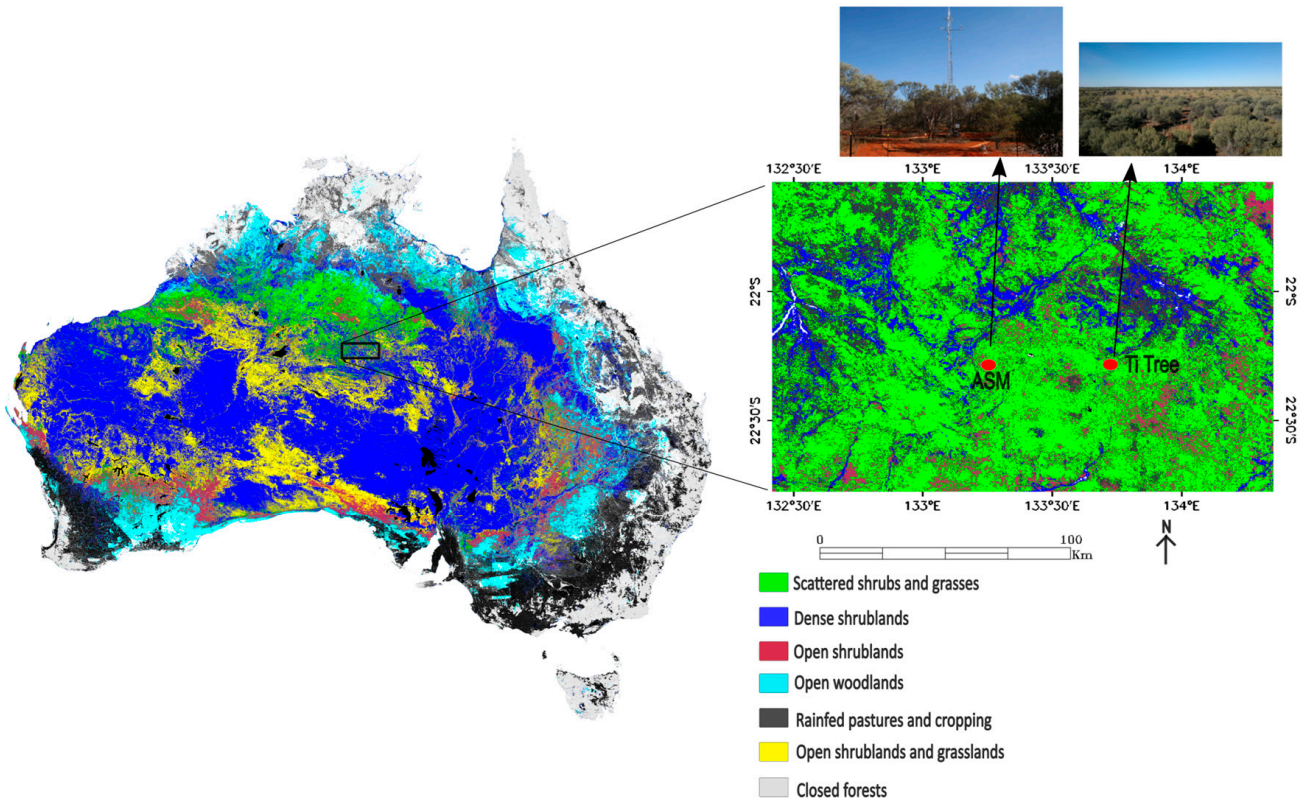

Figure 1. Map of major vegetation groups showing the location of Alice Springs Mulga (ASM) and Ti Tree Ozflux sites (data source: Dynamic Land Cover Dataset Version 2.1).

The sites are located in a flat terrain (slope = 0.2%); the vegetation is similar in both sites, with high-density perennial Mulga savanna woodland (76% cover) consisting of *Acacia aneura* and *Acacia aptaneura* [33]. Ti Tree is characterized by a Mulga (*Acacia aneura*) canopy with the presence of Corymbia. The highest canopy layer has an average height of around 4.8–6.5 m. The grassland and shrub layer is mainly composed of annual and perennial C4 species; the growth and photosynthesis of this layer strongly depend on rainfall amount and are more active in the summer [14]. During dry periods, the bare soil

surface is more widespread than during wet periods [34,35]. Under wet conditions, the soil–plant system has the capability of a quick response, not only because of evaporation from the surface soil layer but also because of the transpiration of both vegetation layers that together explore surface and subsurface horizons [36].

The regional dominant soil type is red kandosol, with a sandy loam texture (74/11/15% sand/silt/clay) and organic matter content of 1.1% at the surface. An extensive siliceous hardpan is more common in this soil type in ASM, showing spatial variability, and its depth can fluctuate from the surface to more than 1 m. Above the hardpan, there is unconsolidated soil. Changes in hardpan depth produce differences in the subsurface storage of soil water and root development, mainly for *Acacia*, which has a dimorphic root system with deep roots. In these cases, a high concentration of roots can be expected above the hardpan [33]. In ASM, this mainly constitutes a limitation for infiltration during strong rainfall events, favoring soil saturation in deep horizons [14]. Access to groundwater by vegetation is hampered by the hardpan or the deep water table (usually around 49 m in depth) [33]. The soil type in the Ti Tree site is also kandosol, with the main difference being the absence of a hardpan.

2.2. Field Data

Table 1 shows the variables from the Ozflux sites considered in our analysis. In situ daily average SM, LST (K), and GPP were used in the present study and can be accessed from [37]. Quality control was carried out as part of the data delivery process, and details on methods of measurements, corrections, and gap filling can be found in previous studies, such as [37]. SM was measured with TDR probes arranged horizontally in two arrays within different habitats: under Mulga, in bare soil between trees, and beneath Mulga and understory (grass, Mulga, and spinifex in the case of Ti Tree) [33]. The sensors measured volumetric soil moisture content (m^3/m^3) at four depths: 0–10 cm (named SSM), 10–30 cm (named 10 cm), 60–80 cm (named 60 cm), and 100–130 cm (named 100 cm). We considered data from the array under Mulga (the most representative cover type) for both stations, which included the unconsolidated soil (at a 100 cm depth) above the hardpan in ASM. The sensors' calibration for the specific soil type was previously carried out by [14], comparing probe measurements with laboratory analysis of soil texture and bulk density.

Table 1. Sensors and variables from the ASM and Ti Tree OzFlux sites considered in this study.

Instrument Type	Brand	Model/Make	Location (Named)
Volumetric soil moisture	Campbell Scientific	CS616 and CS605 (Campbell Scientific Inc)	0–10 cm (SSM) 10–30 cm (10 cm) 60–80 cm (60 cm) 100–130 cm (100 cm)
Net radiometer	Kipp and Zonen	CNR1 (Kipp and Zonen)	12.2 m from ground level

LST from the station was calculated to test the relationship with SM and to check the correlations obtained from MODIS LST data. For the calculation of LST, upwelling long-wave broad band hemispherical radiances measured by the pyrgeometer CNR1, averaging records from 10:30 a.m. to 2:30 p.m, were considered [38] (Equation (2)). This sensor was located at a 11.6 m height in ASM (9.8 m in the Ti Tree station) and included different cover types.

$$LST = \left(\frac{L_{up} - (1 - \varepsilon) L_{down}}{\varepsilon \sigma} \right)^{\frac{1}{4}} \quad (2)$$

where L_{up} and L_{down} are the upwelling and downwelling longwave radiances (w/m^2), respectively; σ is the Stefan–Boltzmann constant (5.67×10^{-8} W/m^2K^4); and ε is the surface emissivity. ε was calculated as [39] follows:

$$\varepsilon = \varepsilon_v F_c + \varepsilon_s (1 - F_c) \quad (3)$$

where ε_v and ε_s are emissivity values for vegetation (0.985) and bare soil (0.960) [40,41], respectively, and *Fc* is the fractional vegetation cover.

$$F_c = \left(\frac{NDVI_i - NDVI_s}{NDVI_v - NDVI_s} \right)^2 \quad (4)$$

where $NDVI_i$, $NDVI_s$, and $NDVI_v$ are NDVI values for each day, for bare soil (0.11), and for vegetation (0.45), respectively, obtained from the MCD43A4 MODIS product (see Section 2.3). $NDVI_i$ values were obtained from a 3×3 pixel window centered in the station. $NDVI_s$ and $NDVI_v$ were calculated as the minimum and maximum NDVI values for the analyzed data series.

Finally, estimates of daily mean GPP (gC/m^2d) from eddy covariance and meteorological data were considered to test the relationship between field and satellite variables during the wet pulses. These data had previously been processed by different authors for the OzFlux sites (more details are included in [14,34]), including quality control assessment, the removal of outliers, and gap-filling and have been used in several studies [5,11,42].

2.3. Satellite Data

We tested the relationship between remotely sensed LST and the LSWI and tested daily field measurements of SM and GPP to analyze the response of vegetation to SM during wet rainfall pulses. Remotely sensed day LST from MODIS Aqua and Terra products (MYD11A1 and MOD11A1 version 6.1, respectively) at 1 km resolution was considered. These products include atmospherically corrected per-pixel temperature and emissivity values. Surface temperature was also corrected from the emissivity effect.

Given the long series and low data gap of MODIS MCD43A4, this nadir Bidirectional Reflectance Distribution Function (BRDF)-Adjusted Reflectance (NBAR) version 6 dataset was considered to obtain NDVI and then emissivity values for thermal field data correction (Equation (2)). This dataset was produced daily using 16 days of Terra and Aqua MODIS data at 500 m resolution. The product is created daily and represents consistent BRDF retrieval for nadir view and solar noon zenith angle over a 16-day series, with the day of interest weighted as a function of quality, observation coverage, and temporal distance from the day of interest (https://lpdaac.usgs.gov/products/mcd43a4v061/, accessed on 18 December 2024).

On the other hand, for the calculation of the LSWI (Equation (5)), we used reflectance data from the recent Japanese Himawari-8 GEO satellite, which carries the AHI, giving a temporal resolution of 10 min. As mentioned, GEO satellites have the advantage of consistency in geometry observation. However, Ref. [5] demonstrated the incidence of sun angle variations on the NDVI and EVI from the AHI, reporting that this effect caused more than one week of uncertainty in retrieving most phenological metrics in South-eastern Australia. In our study, seasonal and spatial variations in sun angles were considered through a BRDF model [43,44]. Daily reflectance (averaging records from 10:30 a.m. to 2:30 p.m.) data were obtained at 10 km resolution adjusted to a solar zenith angle = 45°and view zenith angle = 0°. In spite of the spatial resolution, this dataset was considered because of the comprehensive temporal coverage spanning from 1 August 2017 to 28 May 2022. This extended time period offers potential to test wet pulses of different magnitudes

in comparison with previous AHI non-BRDF corrected datasets. In addition, Ref. [11] reported that the correlation between the GPP and EVI in ASM was almost constant with footprints of satellite observations from 0.25 km to 35 km, showing the small improvement of using a better spatial resolution. In addition, the tower site was located in an extensive homogeneous cover of Mulga woodland [34].

The LSWI, as a spectral index of vegetation water status [24,45,46], was calculated as follows:

$$LSWI = \frac{\rho_{NIR} - \rho_{SWIR}}{\rho_{NIR} + \rho_{SWIR}} \quad (5)$$

where ρ is the surface reflectance in NIR (band 4 of AHI Himawari 8, 0.85–0.87 µm) and SWIR (band 5 of AHI Himawari 8, 1.60–1.62 µm). The index has a generalized equation based on the normalized difference between NIR and SWIR, with this last band being the main indicator of vegetation water status [24]. This index takes values between −1 and 1. Typically, negative values are observed on bare soils or sparse vegetation cover, being almost equal to 0 in humid soil; values increase in the function of vegetation cover and vegetation water content [24].

The EVI was calculated [5,47] as follows:

$$EVI = 2.5\frac{\rho_{NIR} - \rho_{RED}}{\rho_{NIR} + 6\rho_{RED} - 7.5\rho_{BLUE} + 1} \quad (6)$$

where ρ is the reflectance in NIR (band 4 of AHI Himawari 8, 0.85–0.87 µm), RED (band 3 of AHI Himawari 8, 0.60–0.68 µm), and BLUE (band 1 of AHI Himawari 8, 0.49–0.53 µm) bands, respectively.

As in the case of emissivity calculation, satellite data averaged within a 3 × 3 kernel size centered in the stations were extracted for the study period in order to compare them with station measurements. It should be noted that the EVI has been more frequently used in semi-arid Australia, and previous studies have reported a close correlation between that index and GPP [18,42]. Thus, the EVI was calculated as a secondary index just for comparison with the results obtained from the LSWI, and it was considered as an established indicator of vegetation growth and vegetation productivity. Cloud cover was masked out for all of the considered data. Figure 2 shows a flowchart of the analysis carried out.

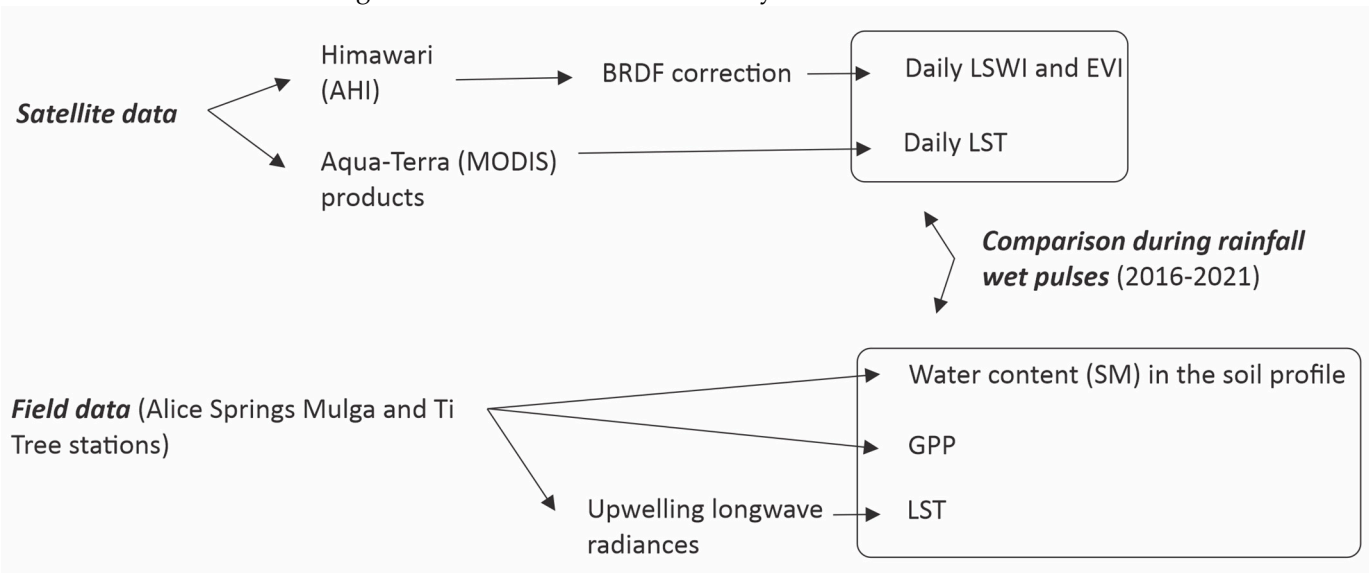

Figure 2. Workflow diagram of satellite data (AHI and MODIS) and field data. Both data sources were considered to obtain LST and spectral indices and analyze vegetation response to SM during rainfall wet pulses.

3. Results

3.1. GPP, Spectral Indices, and SM During the Study Period

Figure 3a shows tower-based GPP and SM at different depths for the study period in ASM. Wet pulses during late spring and summer periods were considered, given that rainfall generally occurs in these seasons (Figure 3b). Different hydrological conditions were covered, similar to those expected for the study area according to the last 20 years series—extremely wet (2016–2017, 2020–2021), normal (2017–2018, 2019–2020), moderately dry (2018–2019) periods. The summer of 2018–2019, when no wet pulses were observed, was included as a dry season to evaluate contrasting hydrological conditions. During both of the wettest periods, significant increases in SM at 60 and 100 cm depths were observed; values around 0.5 m^3/m^3 in deep horizons are mainly due to the existence of a hardpan that favors a high degree of saturation in the soil during extreme events [33]. In the Ti Tree site, data were more limited, but a lower increase in SM in the soil profile is evident (Figure A1a) with similar rainfall amounts (Figure A1b), which can be mainly explained by the absence of a hardpan.

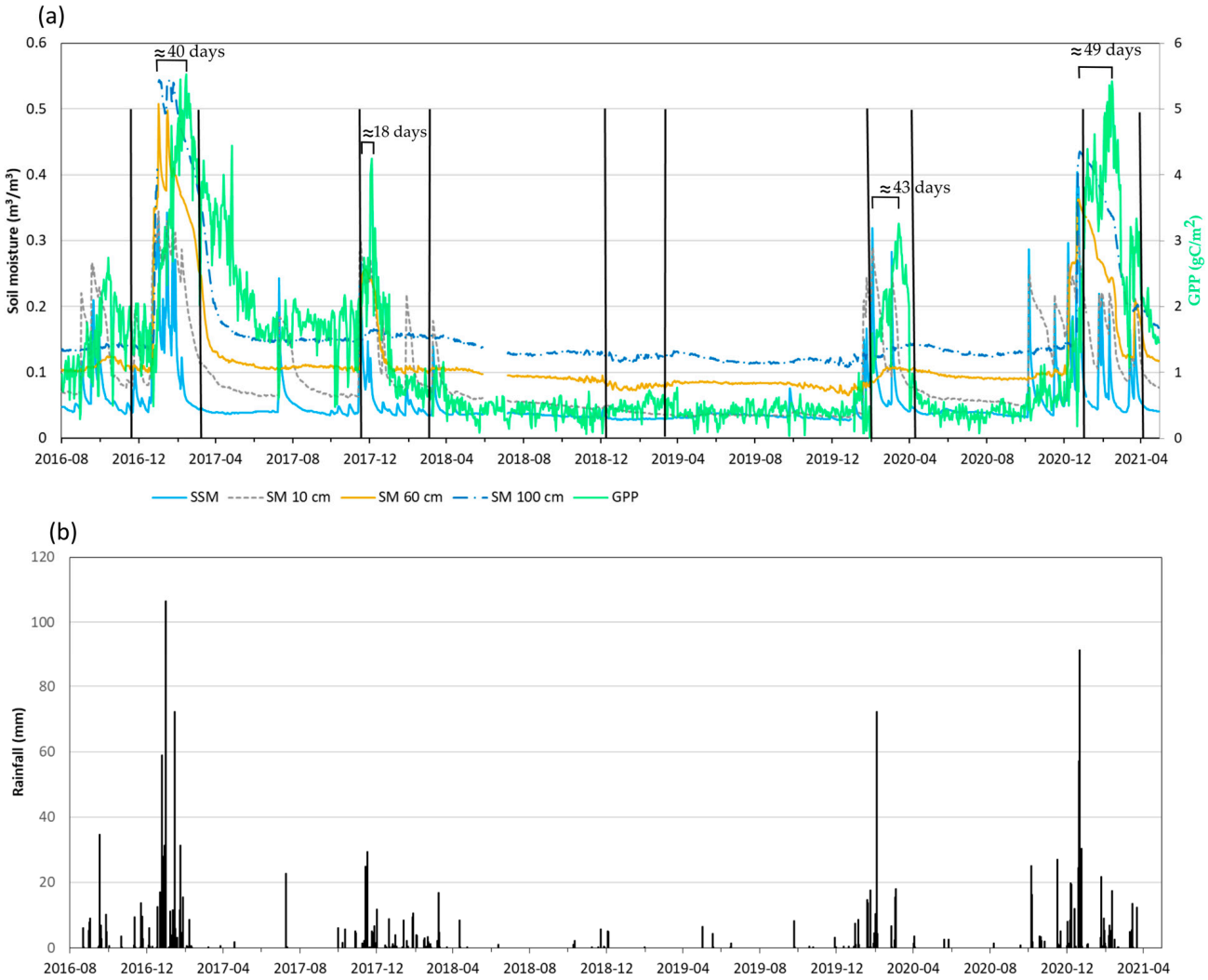

Figure 3. *Cont.*

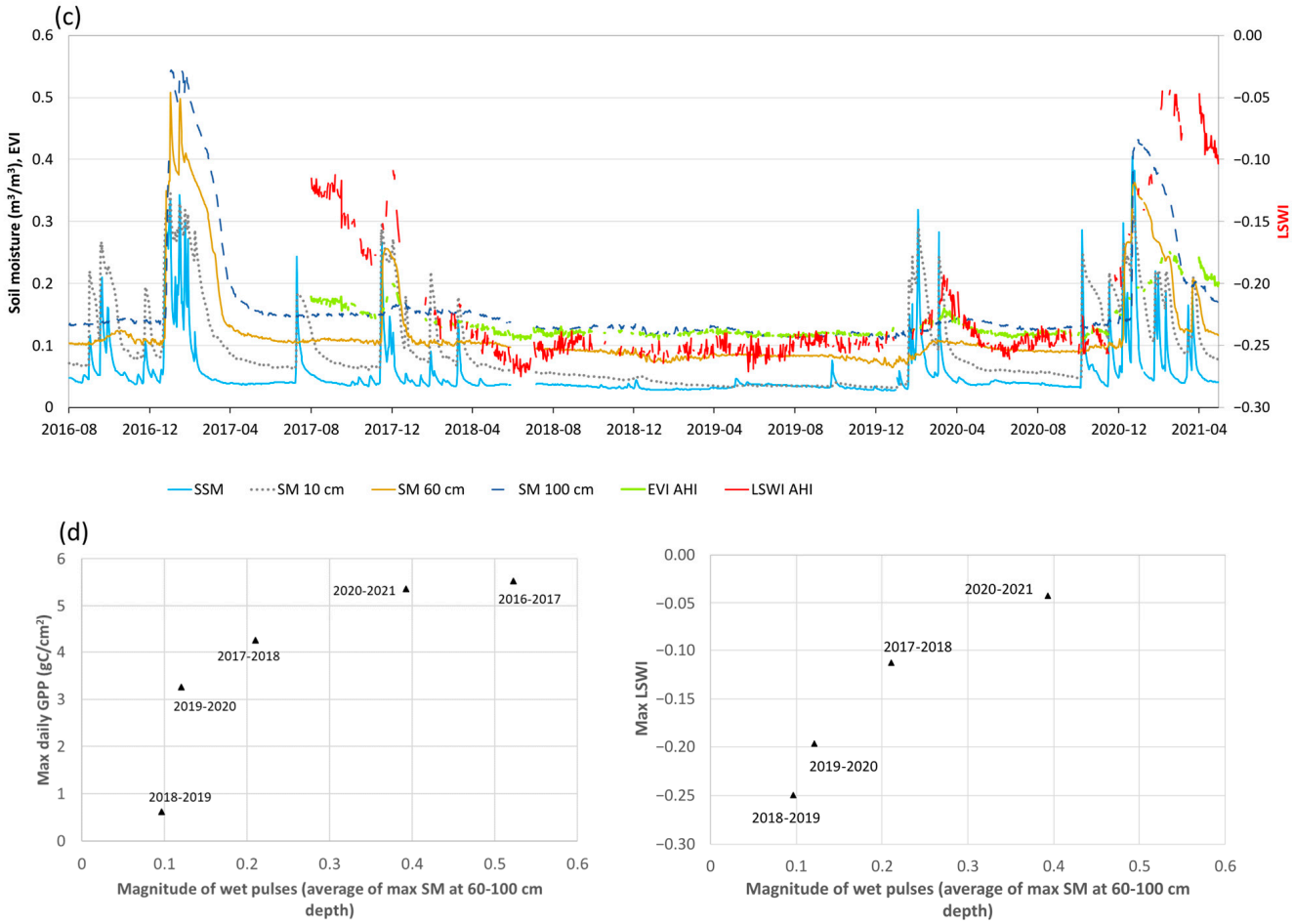

Figure 3. Study periods, data from the ASM OzFlux station. (**a**) Daily SM at different depths and GPP; (**b**) rainfall; (**c**) in situ SM, EVI, and LSWI values from the AHI; (**d**) maximum GPP and LSWI values in function of magnitude of wet pulses expressed as m^3/m^3. Vertical lines show the 5 analyzed wet pulses during late spring and summer: 2016–2017 and 2020–2021, the wettest seasons, and 2018–2019, the driest season.

In general, increases in GPP are strongly related to the magnitude of wet pulses. Rainfall events (around 100–150 mm/week, according to [33]) that recharge SM in deep horizons produce significant increases in vegetation productivity (with maximum GPP values around 5 $gC/m^2/day$). Lags between 18 and 49 days in maximum GPP in relation to peaks in subsurface SM (Figure 3a,d) were observed in ASM. Lags in the Ti Tree station were between 11 and 34 days (Figure A1a).

Figure 3c shows the general behavior of spectral indices for the study period in ASM. It should be noted that the first wet pulse (2016–2017) was not considered because AHI Himawari 8 series was available from mid-2017. The LSWI obtained negative values, consistent with spectral signatures for semi-arid areas that frequently present non-full cover and higher values in SWIR than in NIR bands [24,48]. The general rise in spectral indices is associated with increases in deep SM, with maximum LSWI values associated with the magnitude of wet pulses (Figure 3d). These results are consistent with previous studies carried out in other regions considering the NDVI, the LSWI, rainfall, and drought events [49,50], although studies analyzing SM frequently focus only on SSM (e.g., [51,52]). Low or intermediate pulses (about 0.1–0.2 m^3/m^3), only observed in SSM, did not produce significant increases in spectral indices (e.g., January–March 2018, September–October 2020) (Figure 3c). A comparable pattern was observed in GPP (Figure 3a), given that GPP in the

Mulga woodland is highly correlated with the EVI [53,54]. Similar results were observed in the Ti Tree site, with the seasons with maximum values of the indices and GPP being associated with significant wet pulses (Figure A1c,d).

3.2. Temporal Response of Satellite Information to Wet Pulses

3.2.1. Spectral Indices

A similar pattern in the EVI and LSWI during wet pulses was observed (Figure 4). Certain delays between the maximum in both indices in relation to peaks in SM are evident. Lags between 12 and 40 days between maximum values of SM and LSWI were observed in ASM. In the Ti Tree station, 7 and 31 days for the 2017–2018 and 2020–2021 seasons, respectively, were observed (Figure A1). This daily analysis complements previous studies that considered coarser temporal information. At a monthly scale, Ref. [11] reported delay times from 0 to 1 month in the relationship between SSM and EVI values. Ref. [55] showed a typical delay of 1 month between SM and NDVI values.

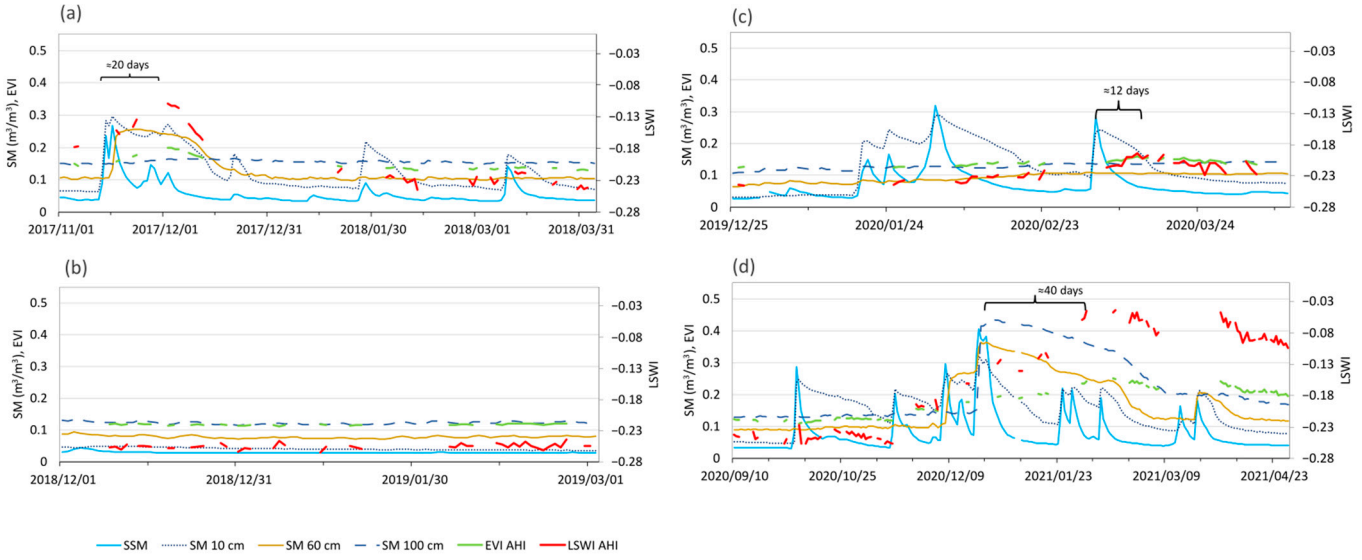

Figure 4. Detailed temporal series of the EVI and LSW from the AHI and SM in ASM for each analyzed season: (**a**) 2017–2018 (normal), (**b**) 2018–2019 (moderately dry), (**c**) 2019–2020 (normal), (**d**) 2020–2021 (extremely wet). Lags between peaks in SM and spectral indices are included.

3.2.2. Land Surface Temperature

Figures 5 and A2 show LST from MODIS, in situ LST and ETa in ASM and Ti Tree, respectively. ETa was estimated by the eddy covariance method (full description in [56]). A typical seasonal pattern in LST with minimum and maximum values in winter and summer, respectively, was observed. For the study periods, a relatively short temporal window between late November to March was considered. Thus, the effect of seasonal changes in LST on the correlations with SM is significantly low. However, this effect should be considered if the entire year is included in the analysis. The results show noticeable decreases during significant wet pulses (end of December 2016–mid-February 2017, December 2020–March 2021) due to evaporative cooling. Using an UAV thermal camera, [33] also reported low sensible heat flux during the summer of wet seasons. Maximum values (336–338 K) were evident in dry summer (February and December 2019). Terra and Aqua showed similar temporal shapes, with lower values from Terra (morning overpass). The general pattern of satellite LST was consistent with field measurements, indicating that satellite information is a good complement to monitor spatial changes in surface energy balance associated with significant wet pulses in this ecosystem. The difference between remotely sensed and in situ LST is explained by the design of the tower and the radiome-

ter (https://www.ozflux.org.au/monitoringsites/alicesprings/alicesprings_pictures.html, accessed on 18 December 2024).

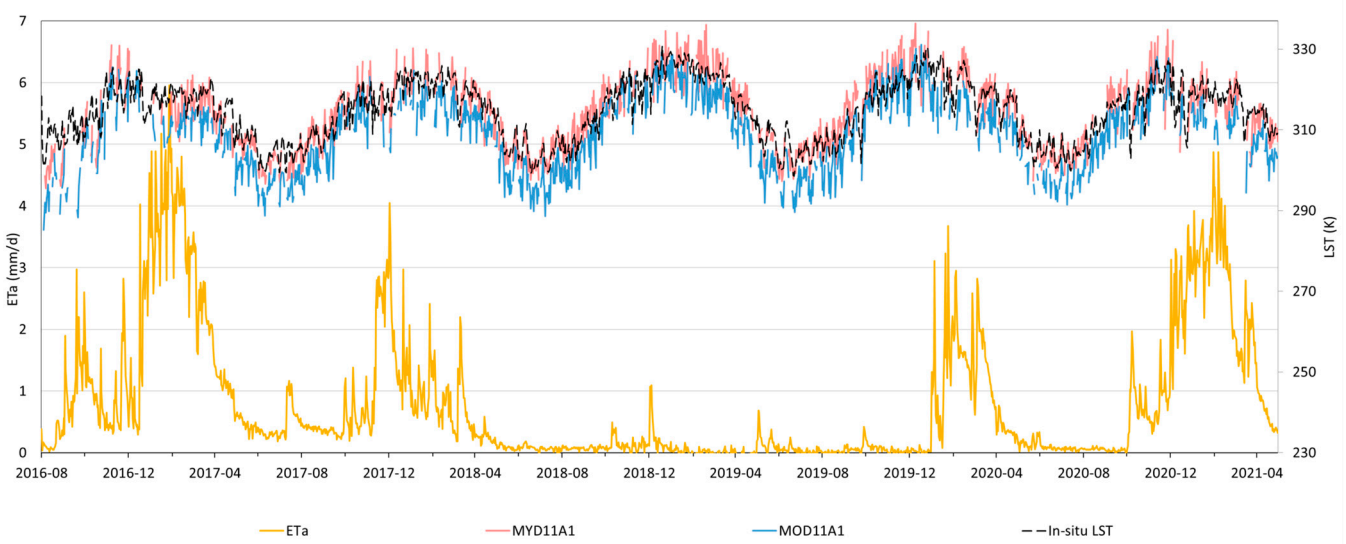

Figure 5. MYD/MOD11A1, in situ daily LST and actual evapotranspiration during the study period in ASM. In situ LST was calculated from upwelling longwave radiances measured by the pyrgeometer CNR1.

Figure 6 shows the detailed temporal series of LST for the studied events in ASM. A quicker response of LST to wet pulses compared to spectral indices can be observed, decreasing the days after the event occurs and maintaining low values during variable temporal windows. That temporal effect of the evaporative cooling process is more noticeable during the wettest pulses (Figure 6a,e), which is associated with increases in ET, as reported by [35] for northern Australia. Those authors showed that vegetation can use available moisture resources rapidly, which can explain the quick fluctuations of LST after significant precipitation events. In general, minimum values (around 305 K) during wet pulses that occur in late spring and summer were observed when deep horizons showed high SM values (10 cm depth: 0.25–0.35 m^3/m^3; 60 cm depth: 0.25–0.5 m^3/m^3; 100 cm: 0.25–0.55 m^3/m^3).

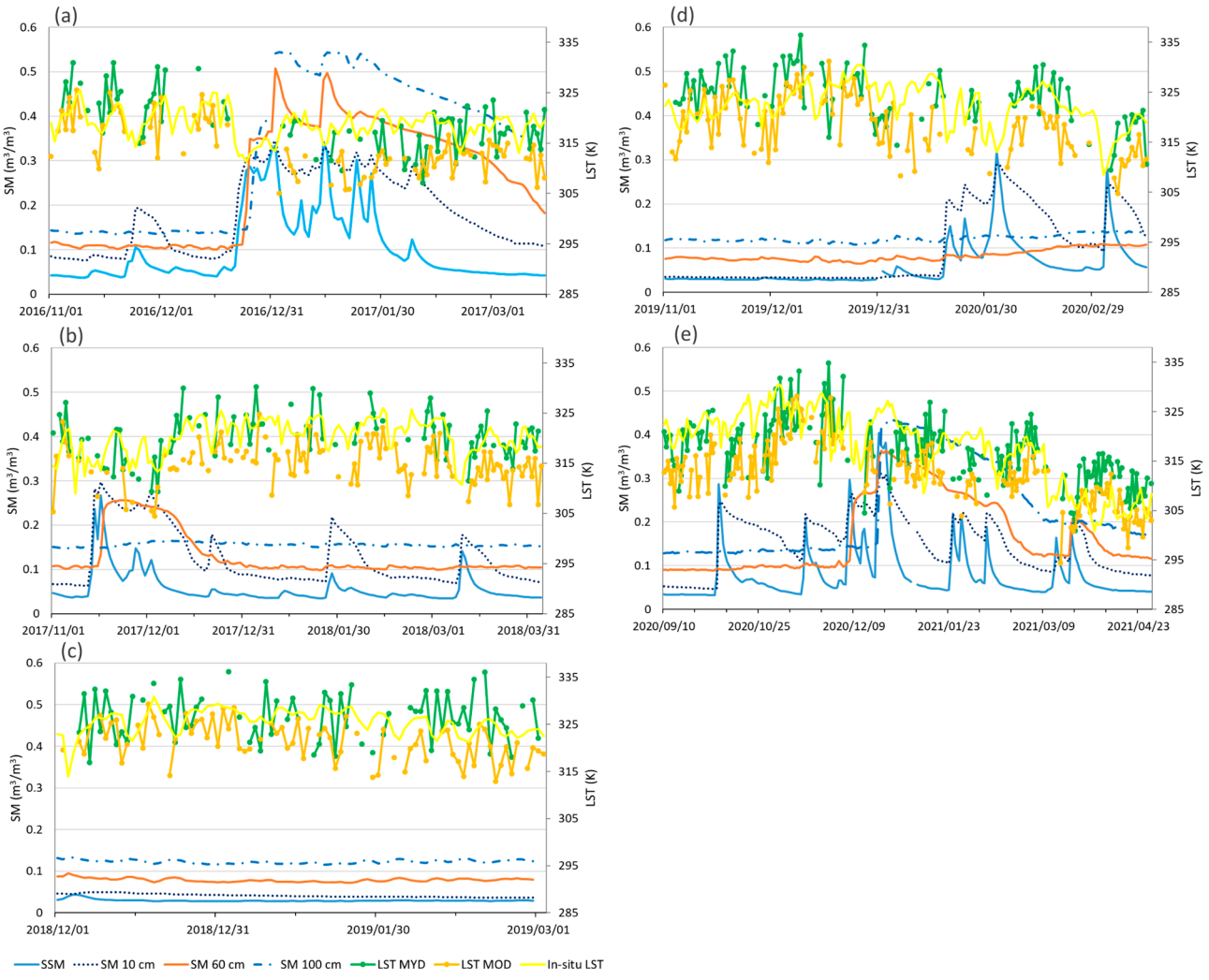

Figure 6. Detailed temporal series of MODIS LST, daily in situ LST and SM in ASM during the 5 analyzed seasons: (**a**) 2016–2017 (extremely wet), (**b**) 2017–2018 (normal), (**c**) 2018–2019 (moderately dry), (**d**) 2019–2020 (normal), and (**e**) 2020–2021 (extremely wet).

3.3. Correlations Between In Situ SM, GPP, and Satellite Information

Figure 7 shows scatter plots between daily SM and spectral indices from the AHI for ASM. The general pattern is similar for both indices, showing a stronger correlation with SM in the deepest considered horizons. Here, the quadratic adjustment is mostly explained by the temporal dynamic of the analyzed variables rather than a causative relationship. That is, SM reaches maximum values quickly in these sandy soils due to low water retention capacity. Those maximums correspond to medium-high values of the indices during the greening stage. Later, maximum values of the indices (a consequence of high ET and antecedent SM) correspond to the decreasing curve of SM (left part of the quadratic regression; see also Figure 3). SSM has a less clear pattern, given the more pronounced fluctuations in that variable (mainly due to strong soil–atmosphere connection and low water retention in the surface horizon) and the vegetation response, mainly to significant wet events. Similar results were observed in the Ti Tree station for both indices (Figure A3), indicating no correlation with surface and 10 cm depth SM and quadratic adjustments for SM at 60 and 100 cm depths ($p < 0.005$).

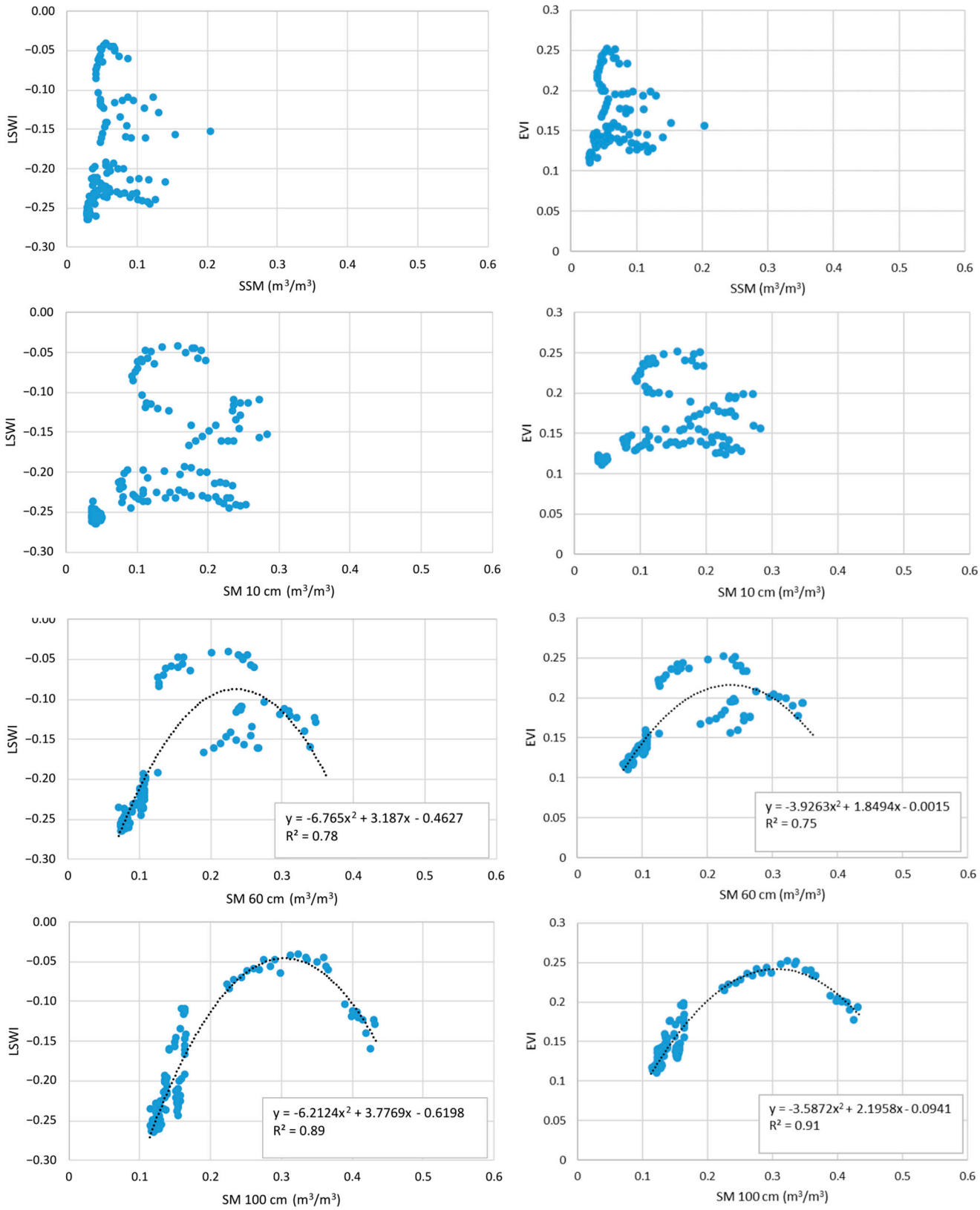

Figure 7. Relationship between daily in situ SM at different depths, LSWI (**left**) and EVI (**right**) from AHI in ASM (n = 356).

Regarding thermal data, in situ LST and SM were considered to evaluate the thermal response of vegetation to soil water content during wet rainfall pulses. The correlation was

tested for the same day and with LST averaged up to 4 days after SM data. Data for rainy dates were removed to avoid noise because of rainfall. Figure 8 shows the scatter plots for ASM with the highest coefficient of determination for that temporal window ($p < 0.005$). The correlation over time suggests the temporal influence of profile soil moisture. A less clear pattern is observed at a 100 cm depth because SM at that depth would have an effect on vegetation mostly during specific periods when the wetting point reaches that depth and/or the hardpan favors soil saturation. Similar results were obtained in the Ti Tree station (Figure A4), showing an asymptotic line for high SM with low correlation at 60 cm and 100 cm depths ($p < 0.005$). These lower correlations can be explained by the less intense increase in SM in deep horizons in the Ti Tree station, with maximum values at 60 and 100 cm depths around 0.16 m^3/m^3 during the analyzed seasons. Contrary to what was observed in ASM, in Ti Tree the absence of the hardpan did not favor the accumulation and permanence of high values of SM (see also Figure 3).

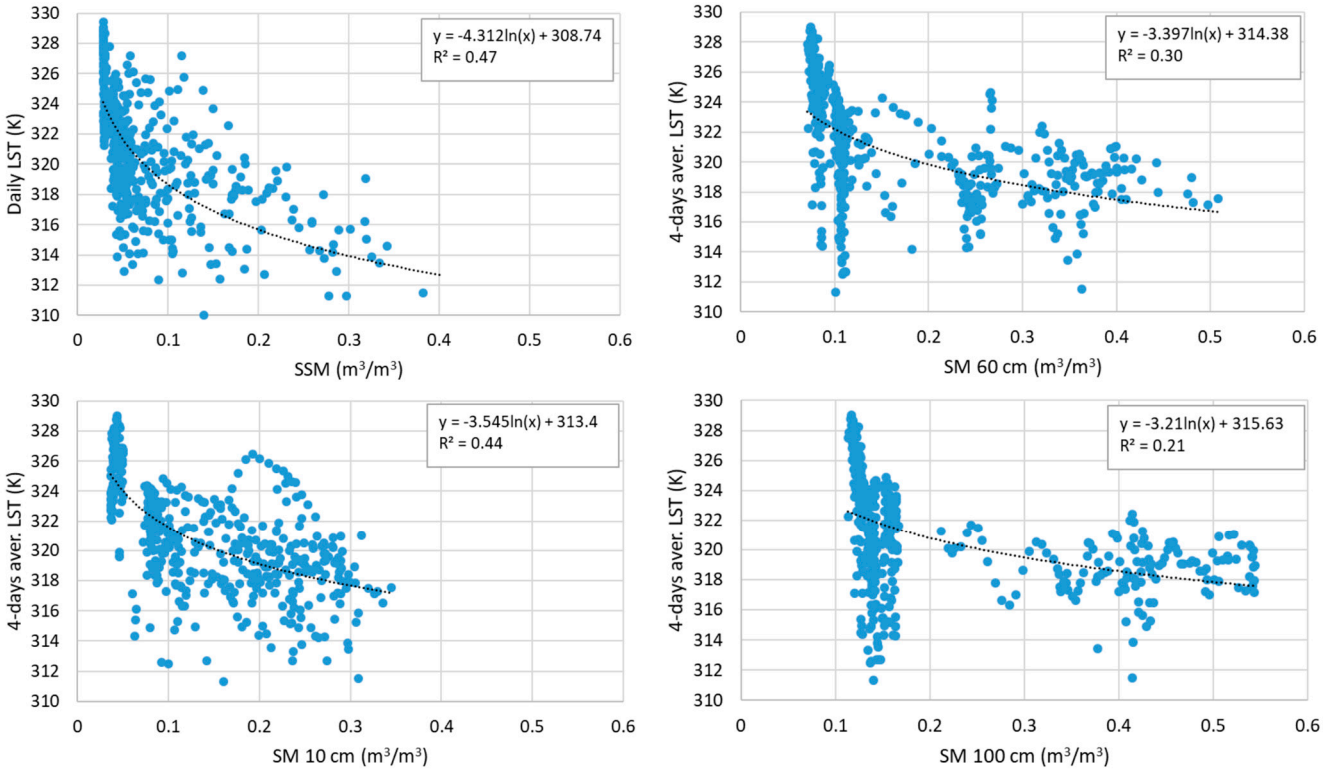

Figure 8. Relationship between average in situ LST and SM at different depths (the best correlation up to 4 days is included) in ASM ($n = 475$). Although correlation at 100 cm depth is included, most of the time LST fluctuates according to shallower SM.

Figure 9 shows the scatter plots between Terra and Aqua LST and daily in situ SM in ASM; rainy days were removed from the analysis. The adjustments and correlations ($p < 0.005$) are consistent with field results (see Figure 8), showing that remotely sensed LST has the potential to reflect the thermal effect of SM on vegetation water conditions during wet pulses. A similar pattern is observed in the Ti Tree station, with a cooling effect of high SM being more evident in the shallow horizons (Figure A5). Given the high ecohydrological sensitivity of these drylands [5,6], a higher correlation might be expected; however, in wet seasons, solar radiation can also be important for vegetation dynamics and atmospheric water demand [57].

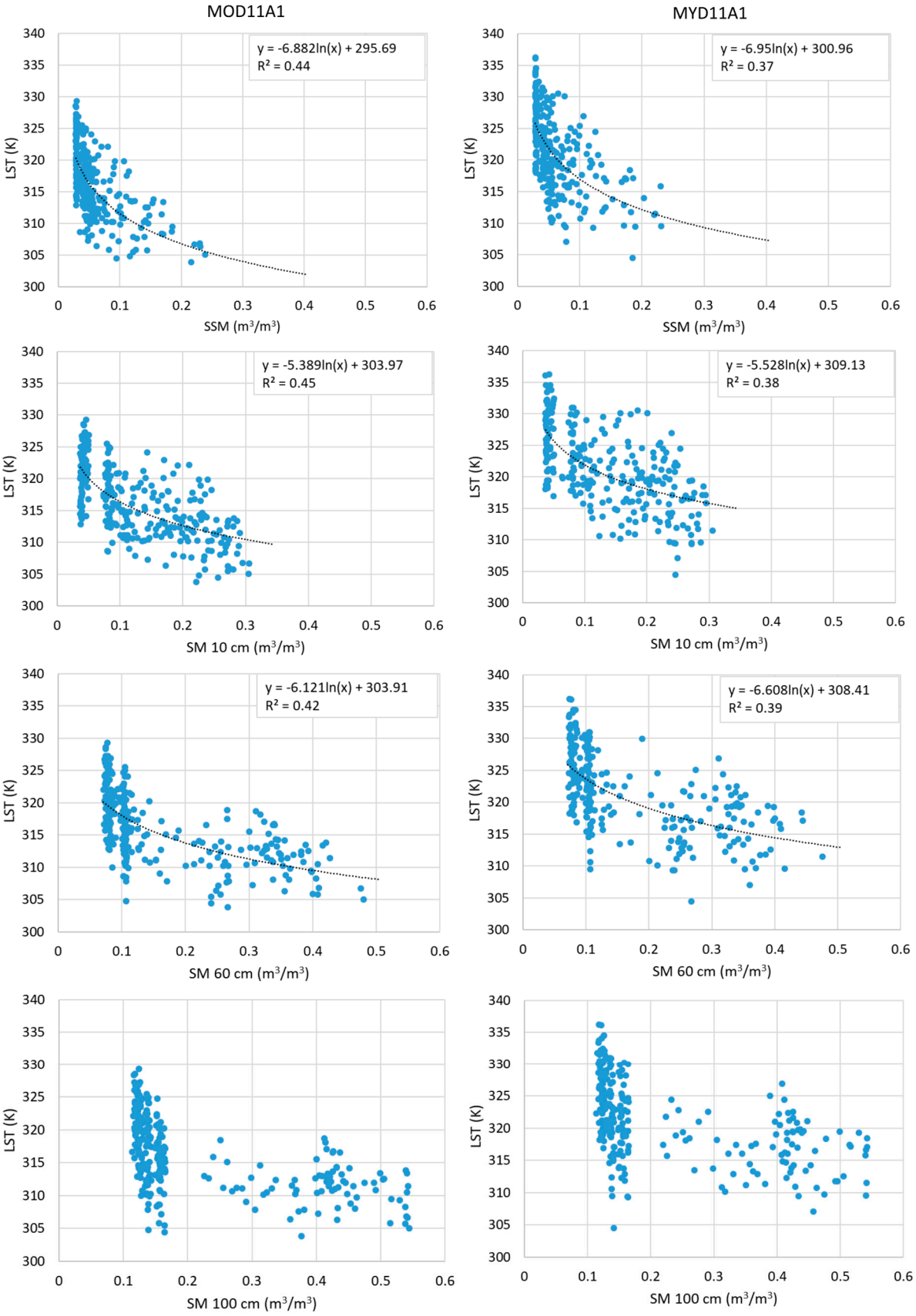

Figure 9. Relationship between daily in situ SM at different depths, MOD11A1 (n = 287) and MYD11A1 (n = 274).

Table 2 shows the correlation between in situ SM and MODIS LST for the same day and the average up to 4 days after from SM data for both stations. The results suggest that increases in SM have an impact on LST for the days following the pulses (also shown in Section 3.2.2). R^2 values were similar at different depths, with no correlation in the Ti Tree station at a 60 cm depth. Regarding the in situ SM/LST relationship, the low correlation in the deepest horizons can be explained by the absence of a hardpan in this station, which does not favor the increase in SM and the extraction of water by plants at those depths.

Table 2. Highest R^2 values ($p < 0.005$) for the relationship between in situ SM and MODIS LST for the same day and the average up to 4 days after, from SM data in the ASM and Ti Tree stations.

SM Depth	R^2 (MOD11A1) ASM	R^2 (MYD11A1) ASM	R^2 (MOD11A1) Ti Tree	R^2 (MYD11A1) Ti Tree
SSM	0.50 (LST 3-day average)	0.46 (LST 2-day average)	0.53 (LST 4-day average)	0.46 (LST 3-day average)
10 cm	0.55 (LST 4-day average)	0.48 (LST 4-day average)	0.49 (LST 4-day average)	0.45 (LST 4-day average)
60 cm	0.49 (LST 4-day average)	0.50 (LST 4-day average)	0.12 (LST 4-day average)	0.00 (LST 4-day average)

With the reflectance data, the association between daily GPP and spectral indices in ASM is shown in Figure 10. The strong correlation present is consistent with previous studies analyzing the EVI at coarser temporal scales in the study region (e.g., [11,58]). Ref. [59] reported relationships between the LSWI from MODIS and the GPP derived from eddy covariance over grassland of Northern China. Ref. [60] found correlations between the EVI and LSWI from MODIS in semi-arid areas of South Africa. We observed a slightly stronger correlation ($p < 0.005$) with the EVI than LSWI (see also Figure A6).

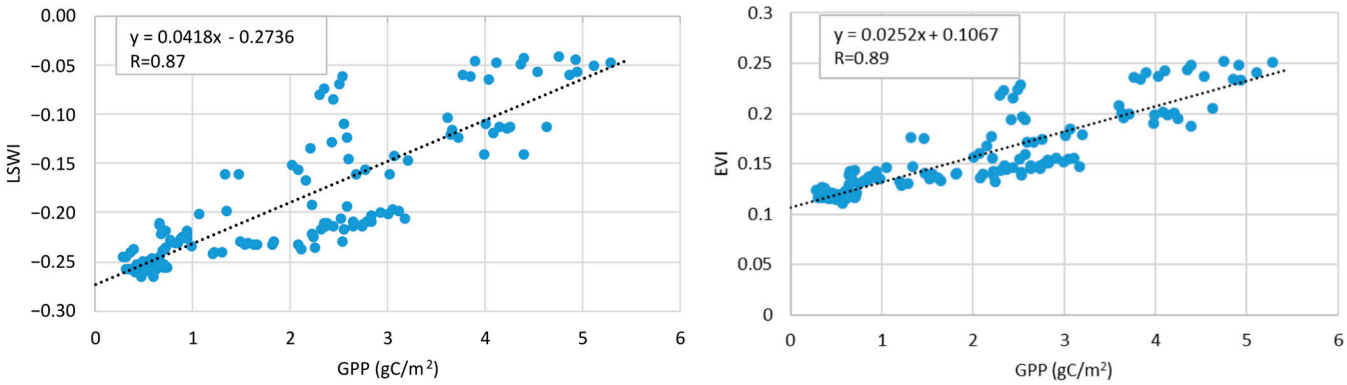

Figure 10. Relationship between daily in situ GPP (gC/m^2), LSWI (**left**), and EVI (**right**) values from the AHI in ASM (n = 145). Note that 2018–2019 was not included, as there was no evident growing season.

Finally, Figure 11 shows the relationship between MODIS LST and in situ daily GPP in ASM. Unlike spectral indices, lower correlations ($p < 0.005$) were observed. This can be explained by the delayed response of GPP in relation to changes in LST related to wet pulses; i.e., GPP is a result of the previous use of water by vegetation. In the Ti Tree station, a low negative relationship was also observed with Terra LST with no correlation with Aqua LST (Figure A7).

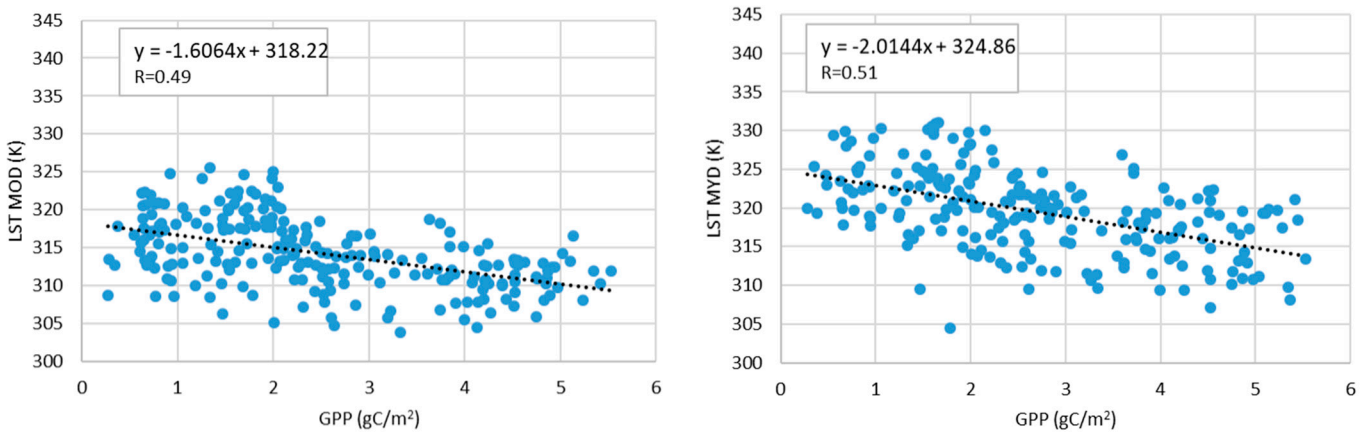

Figure 11. Relationship between daily in situ GPP (gC/m^2), MOD LST (**left**), and MYD LST (**right**) in ASM (n = 232).

4. Discussion

4.1. GPP, Spectral Indices, and SM During the Study Period

The results show that during dry seasons and years, there are no detectable increases in SM and growing seasons, with photosynthetic production being the most minimal during winter (Figure 3) [15]. In general, a quick response of SM at different depths is evident, even more during extremely wet periods, although the decay curve is less steep in deep horizons—typical behavior at depths where the influence of atmospheric water demand decreases (Figure 3a). It should be noted that less important wet pulses produce little changes in SM at 60 or 100 cm depths (e.g., February–March 2020). Ref. [33] reported that precipitations between 0 and 50 mm/week are associated with SM values around 0.10 m^3/m^3 in deep horizons.

The lags between GPP and SM observed in Figures 3 and A1 can be associated with antecedent SM. Refs. [14,33] suggested that subsurface SM acts as a buffer of the dry condition effect between rainfall events. Ref. [33] described how the reserve of water supported root function and small rates of photosynthesis without decreasing phenological and physiological responses to subsequent wet rainfall events. They suggested the existence of a hydraulic lift to shallow roots during dry periods; thus, these roots are maintained, and trees and grasses are synchronized. Then, vegetation has the capability to respond quickly to unpredictable rainfall events. Our results suggest that shorter delays in the response of vegetation to SM pulses can be associated with higher antecedent SM in the deepest horizons that support root systems and the capacity for faster vegetation response, as is the case of the 2017–2018 season.

During dry periods such as in 2018–2019 (Figure 3), there is no clear vegetation growth associated with slight changes in SSM; this is related to the minimum water amount necessary to trigger a response [14]. Ref. [5], analyzing the EVI from MODIS, showed that acacia open woodlands and shrublands have high sensitivity to dry and wet periods. These authors and [35] showed that grass layers strongly respond to rainfall and significantly contribute to GPP during February–March in wet periods; thus, the rapid response of vegetation in late spring and summer should be due to the contribution of both vegetation layers. Some studies have analyzed the partitioning of three-grass functions and structure (e.g., [48,49]), with a detailed discussion of tree and grass contribution to GPP in [5].

The weak response of vegetation to small increases in SSM is consistent with previous studies, like [12], who showed that vegetation in dry climatic zones generally shows great dependence on subsurface SM, especially in the grasslands and shrublands of interior Northern Australia. Some studies have analyzed SM estimates from microwave missions

in the study area [11]. These results suggest that those estimates of SSM could be useful to monitor vegetation response mostly in cases of vertical integration of surface and subsurface SM during significant wet pulses.

4.2. Temporal Response of Satellite Information to Wet Pulses

In general, our results about the temporal response of the LSWI and LST to SM show that the LSWI is an integrative indicator of the cumulative SM effect on vegetation status, but it is not an early proxy of that condition, being temporally associated with the EVI. Changes in vegetation water content have frequently been associated with short-term fluctuations in SM over different vegetation types, given its association with leaf water potential and subsequent extraction of water by the roots. Our results suggest that detectable increases in the satellite-derived LSWI in the study area seem to be strongly associated with the vegetation greenness that can be observed through typical vegetation indices like the EVI. Some studies [25,61] suggest using scatter plots of SWIR/VIs instead of LST/VIs as an indicator of vegetation water condition and SM, given their advantage of better spatial resolution in spectral solar bands. However, considering the observed lags in the response of this spectral index, the use of SWIR over this system should be examined. Although spectral indices associated with changes in vegetation water conditions in the study area should show weekly or daily fluctuations during rainfall wet pulses, sub-daily data can be considered to further test their complementarity with the analyzed temporal scale.

LST has been widely used as an indicator of SM and subsequent ETa through its relationship with evaporative fraction (the ratio between latent heat flux and available energy at the land surface) [29,62]. Several works have explained in detail the behavior of LST indicator of sensible heat flux in relation to physiological processes like stomatal regulation according to soil water content in the root zone and atmospheric water demand (e.g., [63]). Results show decreases in LST in the days after the event occurs, maintaining low values during variable temporal windows (Figure 6). The quick response of LST to wet pulses compared to spectral indices suggests that the temporal effect of the evaporative cooling process is more noticeable during the wettest pulses. Although the sensitivity of this savanna ecosystem is not as large as can be expected in agricultural lands [64,65], where several thermal studies have been conducted, our results suggest that significant decreases in LST during late spring and summer are related to increases in subsurface SM.

4.3. Correlations Between In Situ SM, GPP, and Satellite Information

The correlations between SM, EVI, and LSWI values (Figures 7 and A3) suggest that, although the LSWI has physically been shown to be related to vegetation water content and surface water, both indices showed similar behavior. Field data showed that SM is important for vegetation conditions and productivity. The stronger correlation between GPP and EVI values than LSWI values (Figures 10 and A6) can be explained by the fact that this vegetation index is related to biophysical conditions of vegetation that are more associated with GPP, like photosynthetic pigments and leaf area. In addition, some authors have reported that changes in leaf internal structure, cuticle thickness, and surface characteristics can produce variations in the LSWI unrelated to water content [66,67]. This can be more thoroughly analyzed in future studies.

Regarding thermal data, during wet pulses that increase soil water in deep horizons, vertical integration is expected; thus, soil evaporation can contribute to the cooling process. Likewise, the two vegetation layers can respond quickly to subsurface SM through transpiration [35]. The similar correlations at different depths (Figures 9 and A5) suggest the evaporative cooling effect on the soil–plant system due to increases in SM. In these

savanna woodlands, there can be a combination of a layer of bare soil and two layers of vegetation, and the considered pixel size includes those three ground covers. Thus, the changes in surface energy balance associated with ET should explain the general pattern in the adjustments, where an asymptotic line for high SM and minimum LST values can be deduced. It should be noted that both sites contain a high-density Mulga woodland (76% cover). Thus, the consistent decrease in LST associated with increases in subsurface SM is mainly related to the effect on vegetation. It was not possible to analyze the differentiated effect of soil evaporation on LST from in situ data, given that SSM was not measured on bare soil in both stations.

In general, a clearer pattern can be seen in SSM up to 60 cm in depth (Figure 9). This is consistent with [33,36], who showed that between 65 and 70% of biomass root is found in the upper 30 cm of soil and high concentration of roots in the first 10 cm of the soil. Reference [68] reported that the remaining roots (*Acacia aneura* has a dimorphic root system) can extract deeper SM, which would explain the influence of SM in deeper horizons. More noticeable thermal inertia can be deduced in case of high values of water content ($\geq$0.15 and 0.2 m^3/m^3 at the surface and 10 cm in depth, respectively; $\geq$0.25 m^3/m^3 at 60–100 cm depth in ASM) and, hence, ET. On the other hand, higher thermal amplitude is observed in dry periods, showing that LST depends on other factors. MOD11 LST showed a slightly higher correlation than afternoon overpass, suggesting that ET is better coupled during the morning, and, during the afternoon, the ET may be decoupled because of a mulching effect over SSM.

4.4. General Conceptual Model of LST, SM, and Vegetation Productivity

Under homogeneous atmospheric conditions that determine similar water demand and under comparable incoming solar radiation, LST has been widely associated with SSM (e.g., [29,69]). Not many studies have shown the effect of root zone SM on stomatal resistance to transpiration and evaporative cooling, i.e., ET and then thermal inertia [27,30,63]. Based on our results from in situ SM, GPP, and satellite LST, a general model of the relationship among those variables can be proposed (Figure 12), which has some differences from those previous works that reported linear relationships between SM and LST/optical indices. Given the homogeneous woodland cover in the study area [11], this model can be considered in order to spatially understand the effect of root zone SM on the vegetation status for this ecosystem. SM in the soil profile after significant wet pulses shows the incidence on ET and a cumulative effect on surface energy balance and the subsequent low LST associated with thermal inertia (B in Figure 12, left). That inertia can be considered the resistance of the land surface to thermal variations, being higher in wet surfaces than in dry soil/vegetation and displaying lower temporal temperature fluctuations associated with soil evaporation and transpiration under not limiting conditions. With a certain lag, the LSWI increases and GPP reaches its maximum values, suggesting a plateau for the highest SM in subsurface soil horizons (Figure 12, right). Differences in SM in Figure 12 (right) are mainly explained by the existence of a hardpan in ASM. The impact of rainfall on GPP in Mulga woodlands has been previously reported in different studies [11,33,34]; SM can be a valuable complement to rainfall data, given that it is a more integrative variable of the soil water balance. Figure 12 (right) also suggests the high sensitivity of Mulga woodland productivity to soil water availability, which is consistent with the high reliance of vegetation on subsurface soil water reported for semiarid lands of Central Australia [12,70]; increases in this variable during the wettest periods can produce GPP values up to 5 times higher than those during dry seasons, which is consistent with rainfall amounts and the impact on productivity previously reported [5,33,71]. In Mulga woodlands, asymptotic adjustment suggests a minimum LST for late-spring and summer for

high and extremely high SM that may be associated with thermal regulations of this ecosystem and can be more thoroughly explored in future studies.

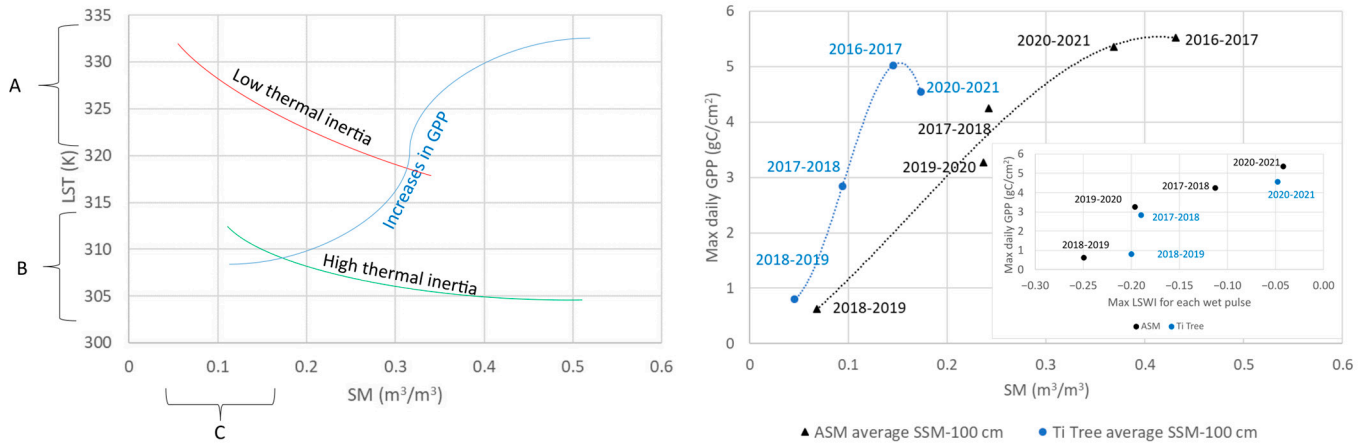

Figure 12. Conceptual model of satellite-derived LST from MODIS (**left**) and daily in situ GPP (**right**) as a function of daily SM for the Mulga woodland area. For the GPP plot, the maximum GPP values and average of the maximum values of SM in the soil profile for each analyzed pulse were considered. GPP versus maximum LSWI from the AHI is included. Note that on the left plot, SM values correspond to ASM data (a similar pattern was observed in Ti Tree).

Furthermore, low–intermediate SM is associated with low thermal inertia (A and C, Figure 12, left); wet pulses that produce a slight increase in shallow SM have a low impact on vegetation productivity (Figure 12 right). Short-term fluctuations in LST, and not directly related to SM, were observed under this condition. Sub-daily analysis can improve the understanding of these fluctuations, whose contributions are probably more associated with heatwaves through land–atmosphere feedback processes or flash drought monitoring than the impact on vegetation productivity, given that during dry periods, such as the 2018–2019 season, vegetation did not show significant growth.

Root zone soil moisture available for plant use has a key role in vegetation conditions in drylands, given that it strongly determines ETa and produces changes with a certain memory depending on the magnitude of rainfall pulses, vegetation access to water, and soil type, among others. In this sense, it is a scarcely explored variable for the early monitoring of vegetation water condition, given the uncertainties in its estimates. Direct estimations of SM from satellite data are frequently limited to the surface water content (typically 5–10 cm for microwave missions) or total water column (Gravity Recovery and Climate Experiment (GRACE) mission). Thus, the spatial evaluation of root zone soil moisture is difficult. Although optical/thermal sensors can have low data coverage during rainfall events due to cloud cover, our study shows that they are related to volumetric soil water content in depths explored by roots, being associated with the ET process. In this sense, they can be a complement to other existing remote sensing methods for the early monitoring of the SM effect on vegetation conditions. To the best of our knowledge, the integration of LST and LSWI values to develop a conceptual model of their relationship with root zone soil moisture and subsequent GPP in Central Australia has not been carried out. The conceptual model proposed in Figure 12 is consistent with previous studies reporting the high dependence of vegetation on accessible water storage in the drylands of Australia (e.g., [12,55,70,72]). It is useful for monitoring vegetation water status and productivity in the study area, given the high dependence of GPP on root zone soil moisture during rainfall wet pulses. This usefulness is especially important in cases of large areas with low coverage from field measurements such as Central Australia, requiring few input data. An important result is the lag in the response of the LSWI (lags between 12 and

40 days in ASM and 7–31 days in Ti Tree between peaks in SM and the maximum index; see Figures 4 and A1) and the early response of LST. This suggests a different potential in cases of use for predicting the impact of SM on vegetation growth and the monitoring of changes in carbon sink associated with the increase in evapotranspiration during significant wet rainfall events.

Certain limitations of this study should be taken into account. The considered region has a slow slope, about 0.2%, and a deep groundwater level, but in areas where water uptake from groundwater is significant, the strong effect of rainfall wet pulses on vegetation can be partially masked.

It should be highlighted that different vegetation responses to SM can be expected according to vegetation sensitivity and root system depth. Thus, correlation parameters can differ from these presented in the analysis, and uncertainties are probably larger for heterogeneous land cover types, taking into account the medium resolution of satellite missions considered in this analysis. It would be of interest to evaluate this distinct response on a regional scale. Although some studies such as [5] reported the differentiated sensitivity of grass and trees to rainfall along the North Australian Tropical Transect, Ref. [33] specifically studied the Mulga woodland around Alice Springs and reported that there are few differences in vegetation growth responses to rainfall between trees and understory grasses. They observed a temporal synchronization between tussock grass understory and Mulga foliage after rainfall pulses. Our study focused on Mulga woodland, the most representative vegetation cover type in the study area. It should be noted that in situ LST measurements covered a mix of different covers (tree, grass, and soil), given the observation angle and the sensor height. Moreover, in situ SM was not measured at different vegetation covers in both considered stations. Considering the spatial resolution of satellite data, it is difficult to differentiate the signal of different vegetation types. However, the relevance of each component can be considered through more detailed in situ studies on LST, soil heat flux, and SM in different vegetation types and in bare soil. Our study was mainly focused on the contribution of satellite data for the integrated monitoring of the system.

Different types of soil can affect the SM available for plants, water balance in the soil, and subsequent vegetation conditions. Thus, although different soils can affect the relationships between optical/thermal data and direct measurements of SM [30], these remote sensing data have the potential to reflect the effect of soil water available for evapotranspiration on vegetation. The study area is an extensive and relatively homogeneous sand plain, being the main type of soil covered by the stations considered in this analysis [33]. Future comparison covering other semi-arid ecosystems can be useful for an intensive study of the interaction between these variables.

Our study aimed to understand the impact of root zone SM during wet rainfall pulses on vegetation in semi-arid Mulga woodland through an integration of in situ measurements and optical/thermal satellite data. Future studies can explore the integration of multi sensors onboard satellites to evaluate scale effects on results. Lastly, the results suggest that the vegetation in Mulga woodland has a weak response to soil water availability during normal rainfall events (i.e., there is LST variability regardless of the few changes in SM). Most of the time, systems such as the Australian drylands are exposed to warm-to-hot annual temperatures and pronounced dry seasons. Mulga woodland has a tolerance to low water potential and efficiently uses SM [14]. The response of semi-arid vegetation to rainfall events generally occurs when the rainfall amount is larger than a threshold that would produce increases in evapotranspiration [14,15]. Under this threshold, variations in LST are mainly associated with factors other than SM. More analyses are needed in the future to explore factors affecting surface energy balance in normal-to-dry periods.

5. Conclusions

In this study, the response of vegetation to in situ root zone soil moisture during wet rainfall pulses in Mulga woodland of semi-arid Central Australia was analyzed through remotely sensed Land Surface Water Index (LSWI) and Land Surface Temperature (LST) values as indicators of vegetation status. Data from geostationary (AHI Himawari-8) and low-Earth-orbiting (MODIS) satellites were considered. The results show that water content in the soil profile explains most vegetation growth seasonally and interannually. Thus, exploring the satellite-based variables strongly related to water availability in the soil to roots can contribute to assessing the impact of wet conditions on vegetation. Daily data of the LSWI displayed a good correlation with soil moisture in deep horizons with quadratic adjustments, explained through the lag in vegetation response. GPP was correlated to the LSWI on a daily scale. This index showed results very similar to those obtained with the EVI, although with a greater range of variation. The temporal response showed that the LSWI increased several days after wet rainfall pulses. The results suggest that it seems to be an integrative indicator of the cumulative effect of soil moisture on vegetation status and productivity, but it is not an early indicator of that condition.

LST showed sensitivity to shorter-term changes in soil profile water content available for evapotranspiration process. In general, the good correlations between soil moisture and LST suggest that LST can be useful for the early monitoring of the vegetation status in the semi-arid ecosystems of the study area during extreme wet events. A general model of LST, according to subsurface water availability, was proposed for the Mulga woodland area. Given the strong association between GPP and soil water in Central semi-arid Australia reported in previous studies, this conceptual framework can be valuable in studies analyzing droughts, vegetation resilience, and productivity. This may become even more relevant in the context of projected increases in the occurrence of extreme events under climate change.

Future studies can analyze the incidence of soil moisture during wet pulses on the growth of different vegetation layers (grassland and shrubland) and the different time responses. In this sense, increases in surface soil moisture seem to be associated with short-term changes in LST, and strong wet pulses can produce a greater impact on productivity and the spectral response.

Author Contributions: Conceptualization, M.H., R.R. and A.H.; Methodology, M.H.; Investigation, M.H.; Data curation, A.S. and R.R.; Writing—original draft, M.H.; Writing—review & editing, A.H.; Visualization, A.S.; Supervision, A.H.; Funding acquisition, M.H. All authors have read and agreed to the published version of the manuscript.

Funding: This work was supported by Consejo Nacional de Investigaciones Científicas y Técnicas (CONICET) through an External Postdoctoral Fellowship. Data are related to "Terrestrial Ecosystem Research Network (TERN), "Developing best-practice Himawari data products for enhanced sub-daily monitoring of Australia's ecosystems", A. Huete (Lead CI)".

Data Availability Statement: The original contributions presented in this study are included in the article. Further inquiries can be directed to the corresponding author.

Acknowledgments: We are thankful to Terrestrial Ecosystem Research Network's (TERN) OzFlux (especially Jamie Rose Cleverly from James Cook University) for providing field data.

Conflicts of Interest: The authors declare no conflict of interest.

Appendix A

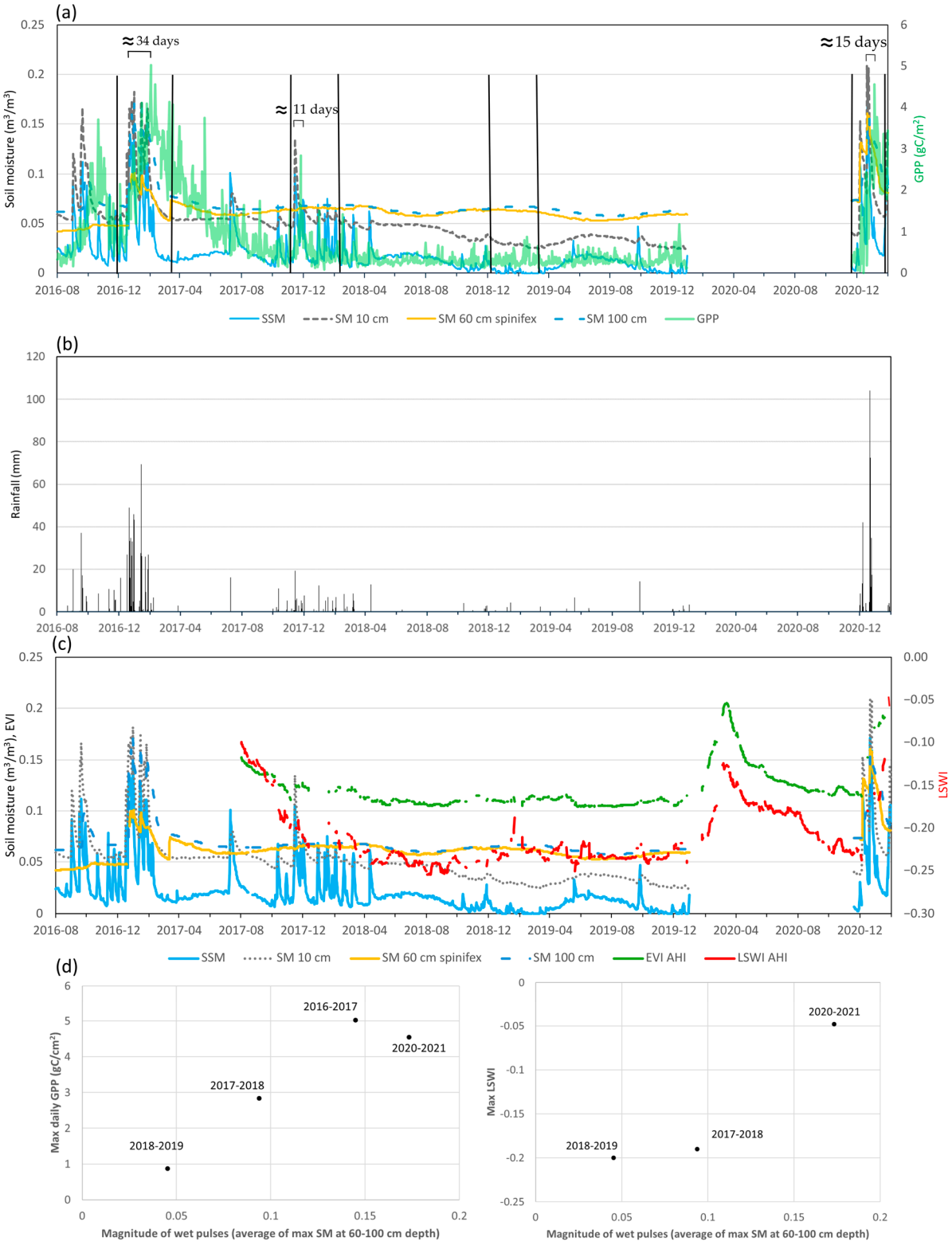

Figure A1. Study periods: data from the Ti Tree OzFlux station. (**a**) Daily SM at different depths and GPP; (**b**) rainfall; (**c**) in situ SM, EVI, and LSWI values from the AHI; (**d**) maximum GPP and LSWI values in function of magnitude of wet pulses expressed as m^3/m^3. Vertical lines show the analyzed wet pulses during late spring and summer. SM at a 60 cm depth was considered under spinifex, given the lack of data under Mulga.

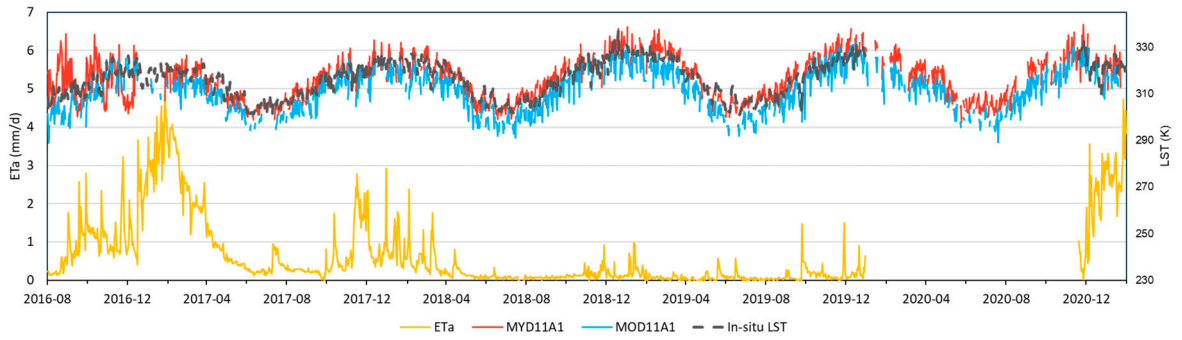

Figure A2. MYD/MOD11A1, in situ daily LST and actual evapotranspiration during the study period in the Ti Tree station. In situ LST was calculated from upwelling longwave radiances measured by the pyrgeometer CNR1.

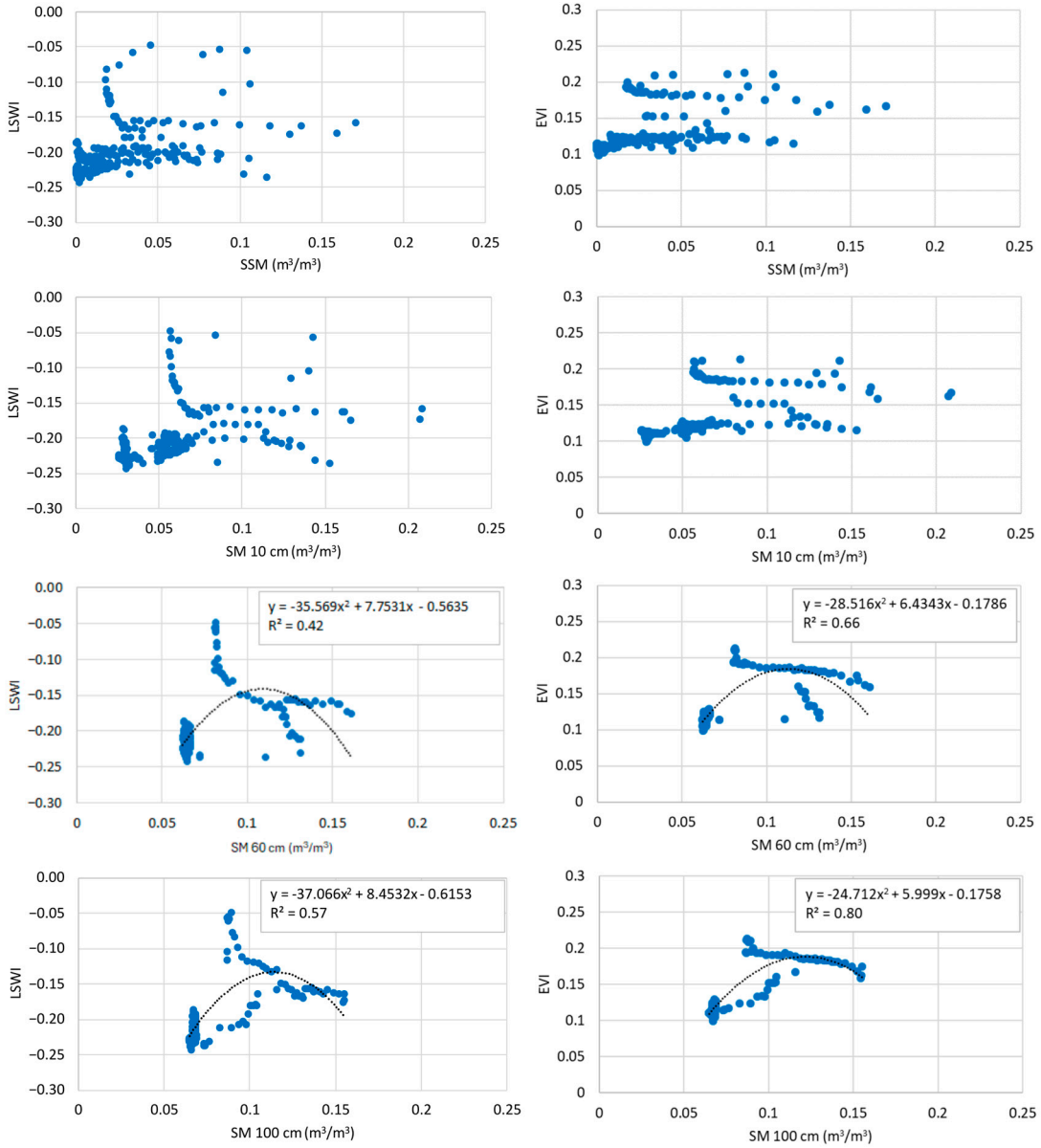

Figure A3. Relationship between daily in situ SM at different depths: the LSWI (**left**) and EVI (**right**) from the AHI in the Ti Tree station (n = 236).

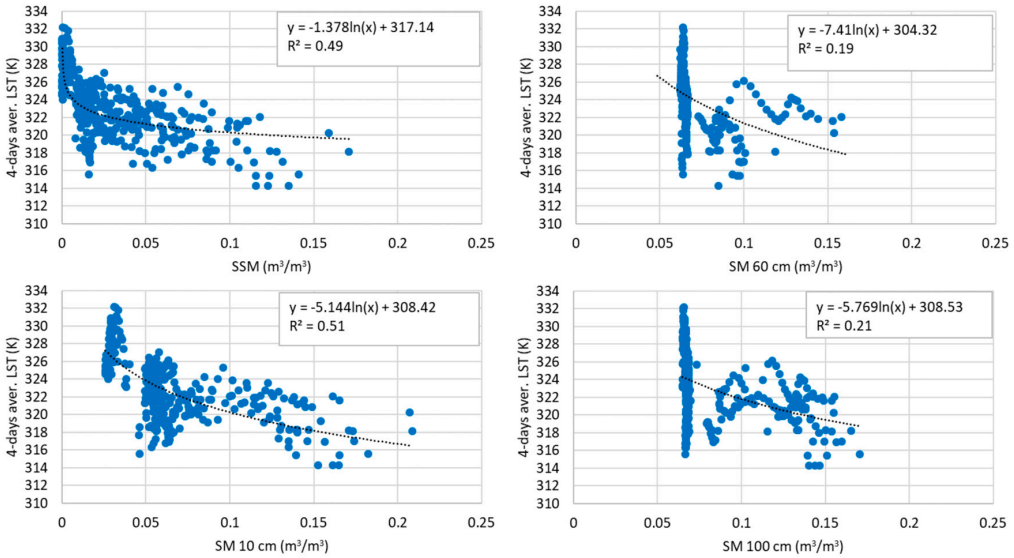

Figure A4. Relationship between average in situ LST and SM at different depths (the best correlation up to 4 days is included) in the Ti Tree station (n = 377).

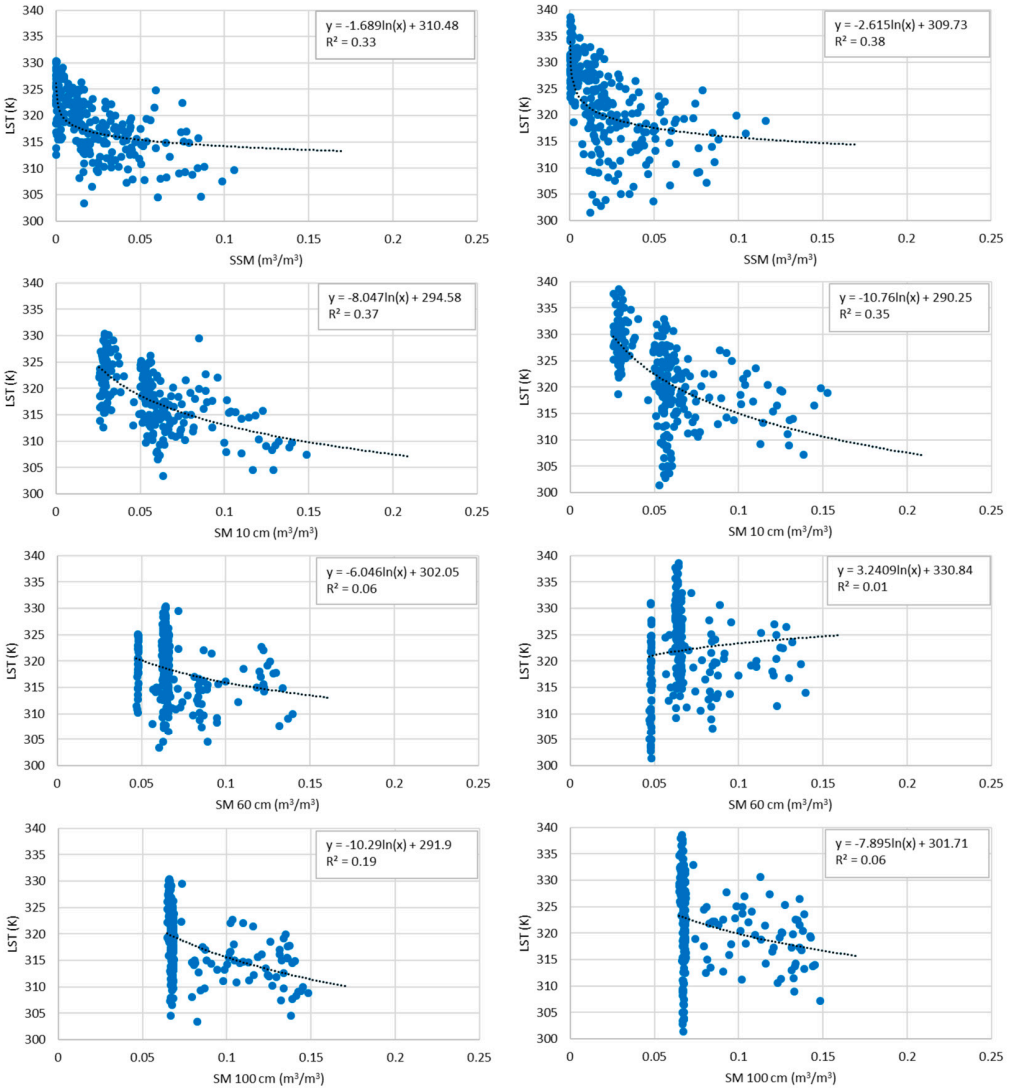

Figure A5. Relationship between daily in situ SM at different depths: MOD11A1 (**left**, n = 251) and MYD11A1 (**right**, n = 239) in the Ti Tree station.

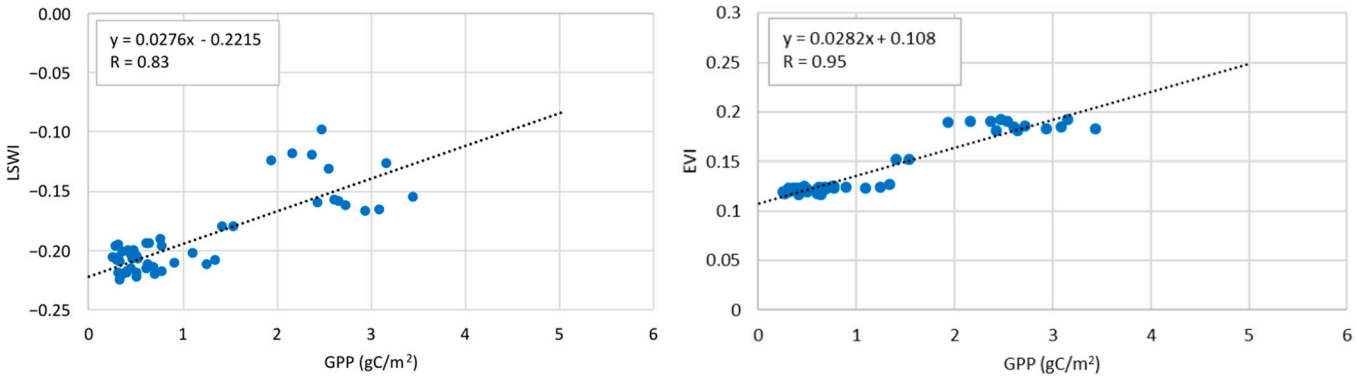

Figure A6. Relationship between daily in situ GPP (gC/m^2), LSWI (**left**), and EVI (**right**) values from the AHI in the Ti Tree station (n = 51). Note that 2018–2019 was not included, as there was no evident growing season.

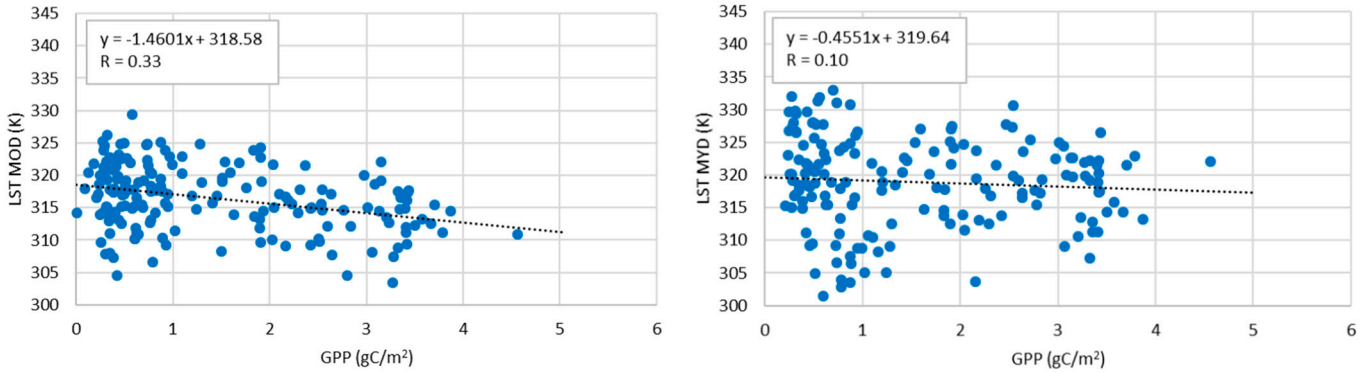

Figure A7. Relationship between daily in situ GPP (gC/m^2), MOD LST (**left**, n = 177), and MYD LST (**right**, n = 169) in the Ti Tree station.

References

1. Detmers, R.G.; Hasekamp, O.; Aben, I.; Houweling, S.; Leeuwen, T.T.; Butz, A.; Landgraf, J.; Köhler, P.; Guanter, L.; Poulter, B. Anomalous Carbon Uptake in Australia as Seen by GOSAT. *Geophys. Res. Lett.* **2015**, *42*, 8177–8184. [CrossRef]
2. Ma, X.; Huete, A.; Cleverly, J.; Eamus, D.; Chevallier, F.; Joiner, J.; Poulter, B.; Zhang, Y.; Guanter, L.; Meyer, W.; et al. Drought Rapidly Diminishes the Large Net CO_2 Uptake in 2011 over Semi-Arid Australia. *Sci. Rep.* **2016**, *6*, 37747. [CrossRef]
3. Rammig, A.; Mahecha, M.D. Ecosystem Responses to Climate Extremes. *Nature* **2015**, *527*, 315–316. [CrossRef] [PubMed]
4. Legesse, T.G.; Dong, G.; Dong, X.; Qu, L.; Chen, B.; Daba, N.A.; Sorecha, E.M.; Zhu, W.; Lei, T.; Shao, C. The Extreme Wet and Large Precipitation Size Increase Carbon Uptake in Eurasian Meadow Steppes: Evidence from Natural and Manipulated Precipitation Experiments. *Environ. Res.* **2023**, *237*, 117029. [CrossRef] [PubMed]
5. Ma, X.; Huete, A.; Moore, C.E.; Cleverly, J.; Hutley, L.B.; Beringer, J.; Leng, S.; Xie, Z.; Yu, Q.; Eamus, D. Spatiotemporal Partitioning of Savanna Plant Functional Type Productivity along NATT. *Remote Sens. Environ.* **2020**, *246*, 111855. [CrossRef]
6. Feldman, A.F.; Short Gianotti, D.J.; Konings, A.G.; McColl, K.A.; Akbar, R.; Salvucci, G.D.; Entekhabi, D. Moisture Pulse-Reserve in the Soil-Plant Continuum Observed across Biomes. *Nat. Plants* **2018**, *4*, 1026–1033. [CrossRef]
7. Ares, M.G.; Holzman, M.; Entraigas, I.; Varni, M.; Fajardo, L.; Vercelli, N. Surface Moisture Area during Rainfall–Run-off Events to Understand the Hydrological Dynamics of a Basin in a Plain Region. *Hydrol. Process.* **2018**, *32*, 1351–1362. [CrossRef]
8. Kumari, N.; Saco, P.M.; Rodriguez, J.F.; Johnstone, S.A.; Srivastava, A.; Chun, K.P.; Yetemen, O. The Grass Is Not Always Greener on the Other Side: Seasonal Reversal of Vegetation Greenness in Aspect-Driven Semiarid Ecosystems. *Geophys. Res. Lett.* **2020**, *47*, e2020GL088918. [CrossRef]
9. Srivastava, A.; Saco, P.M.; Rodriguez, J.F.; Kumari, N.; Chun, K.P.; Yetemen, O. The Role of Landscape Morphology on Soil Moisture Variability in Semi-Arid Ecosystems. *Hydrol. Process.* **2021**, *35*, e13990. [CrossRef]
10. Kooistra, L.; Berger, K.; Brede, B.; Graf, L.V.; Aasen, H.; Roujean, J.-L.; Machwitz, M.; Schlerf, M.; Atzberger, C.; Prikaziuk, E.; et al. Reviews and Syntheses: Remotely Sensed Optical Time Series for Monitoring Vegetation Productivity. *Biogeosciences* **2024**, *21*, 473–511. [CrossRef]

11. Leng, S.; Huete, A.; Cleverly, J.; Lu, X.; Ma, X.; Gao, S.; Yu, Q. Response of Dryland Vegetation under Extreme Wet Events with Satellite Measures of Greenness and Fluorescence. *Sci. Total Environ.* **2022**, *842*, 156860. [CrossRef]
12. Tian, S.; Van Dijk, A.I.J.M.; Tregoning, P.; Renzullo, L.J. Forecasting Dryland Vegetation Condition Months in Advance through Satellite Data Assimilation. *Nat. Commun.* **2019**, *10*, 469. [CrossRef]
13. Fan, Y.; Miguez-Macho, G.; Jobbágy, E.G.; Jackson, R.B.; Otero-Casal, C. Hydrologic Regulation of Plant Rooting Depth. *Proc. Natl. Acad. Sci. USA* **2017**, *114*, 10572–10577. [CrossRef] [PubMed]
14. Cleverly, J.; Boulain, N.; Villalobos-Vega, R.; Grant, N.; Faux, R.; Wood, C.; Cook, P.G.; Yu, Q.; Leigh, A.; Eamus, D. Dynamics of Component Carbon Fluxes in a Semi-Arid Acacia Woodland, Central Australia. *J. Geophys. Res. Biogeosciences* **2013**, *118*, 1168–1185. [CrossRef]
15. Eamus, D.; Huete, A.; Cleverly, J.; Nolan, R.H.; Ma, X.; Tarin, T.; Santini, N.S. Mulga, a Major Tropical Dry Open Forest of Australia: Recent Insights to Carbon and Water Fluxes. *Environ. Res. Lett.* **2016**, *11*, 125011. [CrossRef]
16. Bowman, D.M.J.S.; Boggs, G.S.; Prior, L.D. Fire Maintains an Acacia Aneura Shrubland—Triodia Grassland Mosaic in Central Australia. *J. Arid Environ.* **2008**, *72*, 34–47. [CrossRef]
17. Cleverly, J.; Eamus, D.; Luo, Q.; Restrepo Coupe, N.; Kljun, N.; Ma, X.; Ewenz, C.; Li, L.; Yu, Q.; Huete, A. The Importance of Interacting Climate Modes on Australia's Contribution to Global Carbon Cycle Extremes. *Sci. Rep.* **2016**, *6*, 23113. [CrossRef] [PubMed]
18. Ma, X.; Huete, A.; Moran, S.; Ponce-Campos, G.; Eamus, D. Abrupt Shifts in Phenology and Vegetation Productivity under Climate Extremes. *J. Geophys. Res. Biogeosciences* **2015**, *120*, 2036–2052. [CrossRef]
19. Ma, X.; Huete, A.; Tran, N.N.; Bi, J.; Gao, S.; Zeng, Y. Sun-Angle Effects on Remote-Sensing Phenology Observed and Modelled Using Himawari-8. *Remote Sens.* **2020**, *12*, 1339. [CrossRef]
20. Bhandari, S.; Phinn, S.; Gill, T. Assessing Viewing and Illumination Geometry Effects on the MODIS Vegetation Index (MOD13Q1) Time Series: Implications for Monitoring Phenology and Disturbances in Forest Communities in Queensland, Australia. *Int. J. Remote Sens.* **2011**, *32*, 7513–7538. [CrossRef]
21. Moreno-De Las Heras, M.; Saco, P.M.; Willgoose, G.R.; Tongway, D.J. Variations in Hydrological Connectivity of Australian Semiarid Landscapes Indicate Abrupt Changes in Rainfall-Use Efficiency of Vegetation. *J. Geophys. Res. Biogeosciences* **2012**, *117*, e1839. [CrossRef]
22. Broich, M.; Tulbure, M.G.; Verbesselt, J.; Xin, Q.; Wearne, J. Quantifying Australia's Dryland Vegetation Response to Flooding and Drought at Sub-Continental Scale. *Remote Sens. Environ.* **2018**, *212*, 60–78. [CrossRef]
23. Xie, Q.; Huete, A.; Hall, C.C.; Medlyn, B.E.; Power, S.A.; Davies, J.M.; Medek, D.E.; Beggs, P.J. Satellite-Observed Shifts in C3/C4 Abundance in Australian Grasslands Are Associated with Rainfall Patterns. *Remote Sens. Environ.* **2022**, *273*, 112983. [CrossRef]
24. Holzman, M.E.; Rivas, R.E.; Bayala, M.I. Relationship between TIR and NIR-SWIR as Indicator of Vegetation Water Availability. *Remote Sens.* **2021**, *13*, 3371. [CrossRef]
25. Sadeghi, M.; Jones, S.B.; Philpot, W.D. A Linear Physically-Based Model for Remote Sensing of Soil Moisture Using Short Wave Infrared Bands. *Remote Sens. Environ.* **2015**, *164*, 66–76. [CrossRef]
26. Fensholt, R.; Huber, S.; Proud, S.R.; Mbow, C. Detecting Canopy Water Status Using Shortwave Infrared Reflectance Data from Polar Orbiting and Geostationary Platforms. *IEEE J. Sel. Top. Appl. Earth Obs. Remote Sens.* **2010**, *3*, 271–285. [CrossRef]
27. Holzman, M.E.; Carmona, F.; Rivas, R.; Niclòs, R. Early Assessment of Crop Yield from Remotely Sensed Water Stress and Solar Radiation Data. *ISPRS J. Photogramm. Remote Sens.* **2018**, *145*, 297–308. [CrossRef]
28. Nemani, R.; Pierce, L.; Running, S.; Goward, S. Developing Satellite-Derived Estimates of Surface Moisture Status. *J. Appl. Meteorol.* **1993**, *32*, 548–557. [CrossRef]
29. Nutini, F.; Boschetti, M.; Candiani, G.; Bocchi, S. Evaporative Fraction as an Indicator of Moisture Condition and Water Stress Status in Semi-Arid Rangeland Ecosystems. *Remote Sens.* **2014**, *6*, 6300–6323. [CrossRef]
30. Holzman, M.; Rivas, R.; Bayala, M. Subsurface Soil Moisture Estimation by VI–LST Method. *IEEE Geosci. Remote Sens. Lett.* **2014**, *11*, 1951–1955. [CrossRef]
31. Chang, T.-Y.; Wang, Y.-C.; Feng, C.-C.; Ziegler, A.D.; Giambelluca, T.W.; Liou, Y.-A. Estimation of Root Zone Soil Moisture Using Apparent Thermal Inertia with MODIS Imagery over a Tropical Catchment in Northern Thailand. *IEEE J. Sel. Top. Appl. Earth Obs. Remote Sens.* **2012**, *5*, 752–761. [CrossRef]
32. Morton, S.R.; Stafford Smith, D.M.; Dickman, C.R.; Dunkerley, D.L.; Friedel, M.H.; McAllister, R.R.J.; Reid, J.R.W.; Roshier, D.A.; Smith, M.A.; Walsh, F.J.; et al. A Fresh Framework for the Ecology of Arid Australia. *J. Arid Environ.* **2011**, *75*, 313–329. [CrossRef]
33. Cleverly, J.; Eamus, D.; Restrepo Coupe, N.; Chen, C.; Maes, W.; Li, L.; Faux, R.; Santini, N.S.; Rumman, R.; Yu, Q.; et al. Soil Moisture Controls on Phenology and Productivity in a Semi-Arid Critical Zone. *Sci. Total Environ.* **2016**, *568*, 1227–1237. [CrossRef] [PubMed]
34. Eamus, D.; Cleverly, J.; Boulain, N.; Grant, N.; Faux, R.; Villalobos-Vega, R. Carbon and Water Fluxes in an Arid-Zone Acacia Savanna Woodland: An Analyses of Seasonal Patterns and Responses to Rainfall Events. *Agric. For. Meteorol.* **2013**, *182–183*, 225–238. [CrossRef]

35. Hutley, L.B.; O'Grady, A.P.; Eamus, D. Monsoonal Influences on Evapotranspiration of Savanna Vegetation of Northern Australia. *Oecologia* **2001**, *126*, 434–443. [CrossRef] [PubMed]
36. Jackson, R. B, J.C.; Ehleringer, J.R, Mooney, H.; Sala, O.; Schulze, E. A Global Analysis of Root Distributions for Terrestrial Biomes. *Oecologia* **1996**, *108*, 389–411. [CrossRef] [PubMed]
37. Cleverly, J. Alice Springs Mulga OzFlux Site, OzFlux: Australian and New Zealand Flux Research and Monitoring Network. 2011. Available online: https://data.ozflux.org.au/portal/pub/viewColDetails.jspx?collection.id=152&collection.owner.id=101&viewType=anonymous (accessed on 2 December 2023).
38. Krishnan, P.; Meyers, T.P.; Hook, S.J.; Heuer, M.; Senn, D.; Dumas, E.J. Intercomparison of in Situ Sensors for Ground-Based Land Surface Temperature Measurements. *Sensors* **2020**, *20*, 5268. [CrossRef] [PubMed]
39. Trebs, I.; Mallick, K.; Bhattarai, N.; Sulis, M.; Cleverly, J.; Woodgate, W.; Silberstein, R.; Hinko-Najera, N.; Beringer, J.; Meyer, W.S.; et al. The Role of Aerodynamic Resistance in Thermal Remote Sensing-Based Evapotranspiration Models. *Remote Sens. Environ.* **2021**, *264*, 112602. [CrossRef]
40. Rubio, E.; Caselles, V.; Badenas, C. Emissivity Measurements of Several Soils and Vegetation Types in the 8–14 μm Wave Band: Analysis of Two Field Methods. *Remote Sens. Environ.* **1997**, *59*, 490–521. [CrossRef]
41. Valor, E.; Caselles, V. Mapping Land Surface Emissivity from NDVI: Application to European, African and South American Areas. *Remote Sens. Environ.* **1996**, *57*, 167–184. [CrossRef]
42. Ma, X.; Huete, A.; Yu, Q.; Restrepo-Coupe, N.; Beringer, J.; Hutley, L.B.; Kanniah, K.D.; Cleverly, J.; Eamus, D. Parameterization of an Ecosystem Light-Use-Efficiency Model for Predicting Savanna GPP Using MODIS EVI. *Remote Sens. Environ.* **2014**, *154*, 253–271. [CrossRef]
43. Qin, Y.; McVicar, T.R. Spectral Band Unification and Inter-Calibration of Himawari AHI with MODIS and VIIRS: Constructing Virtual Dual-View Remote Sensors from Geostationary and Low-Earth-Orbiting Sensors. *Remote Sens. Environ.* **2018**, *209*, 540–550. [CrossRef]
44. Qin, Y.; Mitchell, R.; Forgan, B.W. Characterizing the Aerosol and Surface Reflectance over Australia Using AATSR. *IEEE Trans. Geosci. Remote Sens.* **2015**, *53*, 6163–6182. [CrossRef]
45. Ceccato, P.; Gobron, N.; Flasse, S.; Pinty, B.; Tarantola, S. Designing a Spectral Index to Estimate Vegetation Water Content from Remote Sensing Data: Part 2. Validation and Applications. *Remote Sens. Environ.* **2002**, *82*, 198–207. [CrossRef]
46. Fensholt, R.; Sandholt, I. Derivation of a Shortwave Infrared Water Stress Index from MODIS Near- and Shortwave Infrared Data in a Semiarid Environment. *Remote Sens. Environ.* **2003**, *87*, 111–121. [CrossRef]
47. Huete, A.; Didan, K.; Miura, T.; Rodriguez, P.E.; Gao, X.; Ferreira, G.L. Overview of the Radiometric and Biophysical Performance of the MODIS Vegetation Indices. *Remote Sens. Environ.* **2002**, *83*, 195. [CrossRef]
48. Donohue, R.J.; Mcvicar, T.R.; Roderick, M.L. Climate-Related Trends in Australian Vegetation Cover as Inferred from Satellite Observations, 1981–2006. *Glob. Change Biol.* **2009**, *15*, 1025–1039. [CrossRef]
49. Donohue, R.J.; Roderick, M.L.; McVicar, T.R.; Farquhar, G.D. Impact of CO_2 Fertilization on Maximum Foliage Cover across the Globe's Warm, Arid Environments. *Geophys. Res. Lett.* **2013**, *40*, 3031–3035. [CrossRef]
50. Barron, O. *Assessment of the Historical Changes in Groundwater-Dependent Ecosystems (GDEs) in the Peel Region Based on Remote Sensing*; CSIRO: Canberra, Australia, 2020.
51. Khellouk, R.; Barakat, A.; Boudhar, A.; Hadria, R.; Lionboui, H.; El Jazouli, A.; Rais, J.; El Baghdadi, M.; Benabdelouahab, T. Spatiotemporal Monitoring of Surface Soil Moisture Using Optical Remote Sensing Data: A Case Study in a Semi-Arid Area. *J. Spat. Sci.* **2018**, *65*, 481–499. [CrossRef]
52. Huang, C.; Chen, W.; Li, Y.; Shen, H.; Li, X. Assimilating Multi-Source Data into Land Surface Model to Simultaneously Improve Estimations of Soil Moisture, Soil Temperature, and Surface Turbulent Fluxes in Irrigated Fields. *Agric. For. Meteorol.* **2016**, *230–231*, 142–156. [CrossRef]
53. Donohue, R.J.; Hume, I.H.; Roderick, M.L.; McVicar, T.R.; Beringer, J.; Hutley, L.B.; Gallant, J.C.; Austin, J.M.; van Gorsel, E.; Cleverly, J.R.; et al. Evaluation of the Remote-Sensing-Based DIFFUSE Model for Estimating Photosynthesis of Vegetation. *Remote Sens. Environ.* **2014**, *155*, 349–365. [CrossRef]
54. Ma, X.; Huete, A.; Yu, Q.; Coupe, N.R.; Davies, K.; Broich, M.; Ratana, P.; Beringer, J.; Hutley, L.B.; Cleverly, J.; et al. Spatial Patterns and Temporal Dynamics in Savanna Vegetation Phenology across the North Australian Tropical Transect. *Remote Sens. Environ.* **2013**, *139*, 97–115. [CrossRef]
55. Chen, T.; de Jeu, R.A.M.; Liu, Y.Y.; van der Werf, G.R.; Dolman, A.J. Using Satellite Based Soil Moisture to Quantify the Water Driven Variability in NDVI: A Case Study over Mainland Australia. *Remote Sens. Environ.* **2014**, *140*, 330–338. [CrossRef]
56. Cleverly, J.; Eamus, D.; Van Gorsel, E.; Chen, C.; Rumman, R.; Luo, Q.; Coupe, N.R.; Li, L.; Kljun, N.; Faux, R.; et al. Productivity and Evapotranspiration of Two Contrasting Semiarid Ecosystems Following the 2011 Global Carbon Land Sink Anomaly. *Agric. For. Meteorol.* **2016**, *220*, 151–159. [CrossRef]

57. Moore, C.E.; Beringer, J.; Donohue, R.J.; Evans, B.; Exbrayat, J.; Hutley, L.B.; Tapper, N.J. Seasonal, Interannual and Decadal Drivers of Tree and Grass Productivity in an Australian Tropical Savanna. *Glob. Change Biol.* **2018**, *24*, 2530–2544. [CrossRef] [PubMed]
58. Ponce Campos, G.E.; Moran, M.S.; Huete, A.; Zhang, Y.; Bresloff, C.; Huxman, T.E.; Eamus, D.; Bosch, D.D.; Buda, A.R.; Gunter, S.A.; et al. Ecosystem Resilience despite Large-Scale Altered Hydroclimatic Conditions. *Nature* **2013**, *494*, 349–352. [CrossRef] [PubMed]
59. Wang, Z.; Xiao, X.; Yan, X. Modeling Gross Primary Production of Maize Cropland and Degraded Grassland in Northeastern China. *Agric. For. Meteorol.* **2010**, *150*, 1160–1167. [CrossRef]
60. Maluleke, A.; Feig, G.; Brümmer, C.; Rybchak, O.; Midgley, G. Evaluation of Selected Sentinel-2 Remotely Sensed Vegetation Indices and MODIS GPP in Representing Productivity in Semi-Arid South African Ecosystems. *J. Geophys. Res. Biogeosciences* **2024**, *129*, 4. [CrossRef]
61. Sadeghi, M.; Babaeian, E.; Tuller, M.; Jones, S.B. The Optical Trapezoid Model: A Novel Approach to Remote Sensing of Soil Moisture Applied to Sentinel-2 and Landsat-8 Observations. *Remote Sens. Environ.* **2017**, *198*, 52–68. [CrossRef]
62. Holzman, M.E.; Rivas, R.E. Optical/thermal-based techniques for subsurface soil moisture estimation. In *Satellite Soil Moisture Retrievals: Techniques & Applications*; Srivastava, P.K., Petropoulos, G., Kerr, Y., Eds.; Elsevier Science: Cambridge, UK, 2016; pp. 73–89, ISBN 978-0-12-803388-3.
63. Holzman, M.E.; Rivas, R.; Piccolo, M.C. Estimating Soil Moisture and the Relationship with Crop Yield Using Surface Temperature and Vegetation Index. *Int. J. Appl. Earth Obs. Geoinf.* **2014**, *28*, 181–192. [CrossRef]
64. Cleverly, J.; Thibault, J.R.; Teet, S.B.; Tashjian, P.; Hipps, L.E.; Dahm, C.N.; Eamus, D. Flooding Regime Impacts on Radiation, Evapotranspiration, and Latent Energy Fluxes over Groundwater-Dependent Riparian Cottonwood and Saltcedar Forests. *Adv. Meteorol.* **2015**, *2015*, 935060. [CrossRef]
65. Schuepp, P.H. Tansley Review No. 59 Leaf Boundary Layers. *New Phytol.* **1993**, *125*, 477–507. [CrossRef] [PubMed]
66. Buitrago, M.F.; Groen, T.A.; Hecker, C.A.; Skidmore, A.K. Changes in Thermal Infrared Spectra of Plants Caused by Temperature and Water Stress. *ISPRS J. Photogramm. Remote Sens.* **2016**, *111*, 22–31. [CrossRef]
67. Datt, B. Remote Sensing of Water Content in Eucalyptus Leaves. *Aust. J. Bot.* **1999**, *47*, 909–923. [CrossRef]
68. Eamus, D.; O'Grady, A.P.; Hutley, L. Dry Season Conditions Determine Wet Season Water Use in the Wet-Dry Tropical Savannas of Northern Australia. *Tree Physiol.* **2000**, *20*, 1219–1226. [CrossRef] [PubMed]
69. Nutini, F.; Stroppiana, D.; Busetto, L.; Bellingeri, D.; Corbari, C.; Mancini, M.; Zini, E.; Brivio, P.A.; Boschetti, M. A Weekly Indicator of Surface Moisture Status from Satellite Data for Operational Monitoring of Crop Conditions. *Sensors* **2017**, *17*, 1338. [CrossRef] [PubMed]
70. Wang-Erlandsson, L.; Bastiaanssen, W.G.M.; Gao, H.; Jägermeyr, J.; Senay, G.B.; van Dijk, A.I.J.M.; Guerschman, J.P.; Keys1, P.W.; Gordon, L.J.; Savenije, H.H.G. Global Root Zone Storage Capacity from Satellite-Based Evaporation. *Hydrol. Earth Syst. Sci.* **2016**, *20*, 1459–1481. [CrossRef]
71. Porporato, A.; Daly, E.; Rodriguez-Iturbe, I. Soil Water Balance and Ecosystem Response to Climate Change. *Am. Nat.* **2004**, *164*, 625–632. [CrossRef]
72. Yang, Y.; Long, D.; Guan, H.; Scanlon, B.; Simmons, C.T.; Jiang, L.; Xu, X. GRACE Satellite Observed Hydrological Controls on Interannual and Seasonal Variability in Surface Greenness over Mainland Australia. *J. Geophys. Res.* **2014**, *119*, 2245–2260. [CrossRef]